Chemical Engineering Communications
Publication details, including instructions for authors and subscription information:
http://www.tandfonline.com/loi/gcec20

# STEADY STATE AND DYNAMIC MODELLING OF A PACKED BED REACTOR FOR THE PARTIAL OXIDATION OF METHANOL TO FORMALDEHYDE I. MODEL DEVELOPMENT

LARRY C. WINDES [a] , MARVIN J. SCHWEDOCK [a] & W. HARMON RAY [a]
[a] Department of Chemical Engineering , University of Wisconsin , Madison , WI , 53706
Published online: 05 Apr 2007.

To cite this article: LARRY C. WINDES , MARVIN J. SCHWEDOCK & W. HARMON RAY (1989) STEADY STATE AND DYNAMIC MODELLING OF A PACKED BED REACTOR FOR THE PARTIAL OXIDATION OF METHANOL TO FORMALDEHYDE I. MODEL DEVELOPMENT, Chemical Engineering Communications, 78:1, 1-43, DOI: 10.1080/00986448908940185

To link to this article: http://dx.doi.org/10.1080/00986448908940185

*Chem. Eng. Comm.* 1989, Vol. 78, pp. 1–43
Reprints available directly from the publisher.
Photocopying permitted by license only.

Printed in the United States of America



# STEADY STATE AND DYNAMIC MODELLING OF A PACKED BED REACTOR FOR THE PARTIAL OXIDATION OF METHANOL TO FORMALDEHYDE

## I. MODEL DEVELOPMENT

LARRY C. WINDES,‡ MARVIN J. SCHWEDOCK,† and W. HARMON RAY§

*Department of Chemical Engineering*
*University of Wisconsin*
*Madison, WI 53706*

*(Received March 10, 1987; in final form June 7, 1988)*

Several levels of mathematical models involving one and two dimensions as well as single and multiple phases are used to predict the steady state and dynamic behavior of a packed bed reactor for the partial oxidation of methanol to formaldehyde. Parametric sensitivity is examined for several heat and mass transfer parameters, kinetic parameters, and operating conditions. Yield is compared for various models, and significant differences are observed between the one-dimensional and two-dimensional models. The dynamic behavior after step changes in the operating conditions is found to be qualitatively similar for different models.
KEYWORDS Packed bed Model Partial oxidation Formaldehyde.

## INTRODUCTION

The tubular packed bed reactor presents a challenging problem for accurate modelling and control. The detailed model is extremely complex due to the large number of heat, mass, and momentum transfer processes occurring in the reactor. The randomly packed bed of catalyst particles with the fluid flowing around them adds an element of uncertainty to any model, and makes exact mathematical modelling of each catalyst particle impossible. Some difficult factors in developing a good dynamic model for the reactor are:

1. the multi-dimensional distributed configuration,
2. the two-phase nature of the reactor bed,
3. the non-linear dependence of the rate of reaction on temperature,
4. the non-uniformity of the packing and the flow through it,
5. the uncertainty of several of the heat and mass transfer parameters,
6. parameters that vary depending on the location within the reactor bed.

In addition, many chemical species are often present with reactions represented

† Present address: Unocal, Science & Technology, Brea, CA 92621.
‡ Present address: Tennessee Eastman Co., Kingsport, TN 37662.
§ Author to whom correspondence should be addressed.

by complex kinetic expressions having time-varying rates due to catalyst deactivation.

By considering the reactor as a continuum, partial differential equations can be written to account for a large portion of the known phenomena. However, some simplifications must be made before a computational solution faster than real time is feasible. The model must be simple enough so that unknown parameters can be elucidated by appropriate experiment and also accurate enough to indicate the maximum hot-spot temperature and product yield. The present study is distinct from earlier work in that it is concerned with situations where packed bed dynamic behavior has a strong effect on selectivity and product yield. Our goal is a sufficiently realistic reactor model which can be incorporated into a model-based control system which includes on-line yield optimization. The results given in this paper can be readily generalized for other packed bed reactors with moderately exothermic reactions.

A rather general complex mathematical model has been developed which allows for a large degree of flexibility in simplification for specific applications. This versatile reactor simulator is designed to:

1. evaluate the relative importance of various simplifying assumptions,
2. accurately represent results of real reactor experiments,
3. be solved quickly enough to be used in conjunction with real time state estimation and control programs.

Packed bed reactor models described in the literature have usually been substantially simplified at the outset, and few direct comparisons between different types of models have been made. In this work we use our general model to predict the behavior of experimental reactors and then compare the performance of various simplified forms of the model in realistically simulating the reactor. In the sequel (Part II) we describe detailed comparisons of our model with data from a pilot scale reactor in our laboratory.

## EXPERIMENTAL SYSTEM STUDIED

To give the reactor modelling study greater practical importance, a reaction system of industrial significance has been selected. The pilot plant reactor will carry out the partial oxidation of methanol to formaldehyde over a commercial iron-oxide/molybdenum-oxide catalyst. Two major technologies exist for the direct oxidation of methanol with air to produce formaldehyde:

1. The older process based on a silver catalyst, in which the feed is on the methanol-rich side of a flammable mixture,
2. The newer process used in this study based on an iron-oxide molybdenumoxide catalyst with the feed on the methanol-lean side of a flammable mixture.

The principle reaction is

$$CH_3OH + \tfrac{1}{2}O_2 \rightarrow CH_2O + H_2O \quad (-\Delta H) = 37.9 \text{ kcal/mol} \qquad (1)$$

Carbon monoxide is produced in an undesirable consecutive reaction by the partial oxidation of formaldehyde:

$$CH_2O + \tfrac{1}{2}O_2 \rightarrow CO + H_2O \quad (-\Delta H) = 55.7 \text{ kcal/mol} \tag{2}$$

These reactions take place at atmospheric pressure and at 250–400°C. The typical reactor has many tubes of ~1 m in length and 15–25 mm in diameter, and the exothermic heat of reaction is removed by means of a coolant on the outside of the reactor tube. The reactor modelling in this study will consider a single reactor tube as shown schematically in Figure 1.

For a range of the operating conditions, the methanol reaction is limited by diffusion in the catalyst pores, and the observed activation energy of the secondary reaction (2) is higher than for reaction (1). Because of this ratio of activation energies and the high conversion of methanol, there exists an optimum temperature for the maximum yield of formaldehyde from the reactor. As part of the practical part of this study, we shall seek to optimize the reactor with respect to the manipulated variables which control the operation. For the experimental system under study these are:

1. coolant or wall temperature, $T_W$: ~250°C
2. feed temperature, $T_i$: ~250°C
3. feed mole fraction methanol, $y_i$: ~0.05
4. flow rate, $m$: ~1.4 g/sec; $G$: ~2.5 kg/m$^2$ sec

Let us now develop the reaction kinetics to be used. The catalyst is an unsupported $Fe_2O_3$–$MoO_3$ mixture in a weight ratio of 20:80. The conclusion from most of the reported research on the mechanism of methanol oxidation is that the reaction proceeds by a redox mechanism (Dente *et al.*, 1964; Jiru *et al.*, 1964; Machiels and Sleight, 1982; Machiels, 1982). This model was originally proposed for the oxidation of aromatic hydrocarbons on vanadium oxide catalysts (Mars and Van Krevelen, 1954) and has not been qualitatively modified. Methanol reacts with a lattice oxygen to produce formaldehyde, and simultaneously vapor

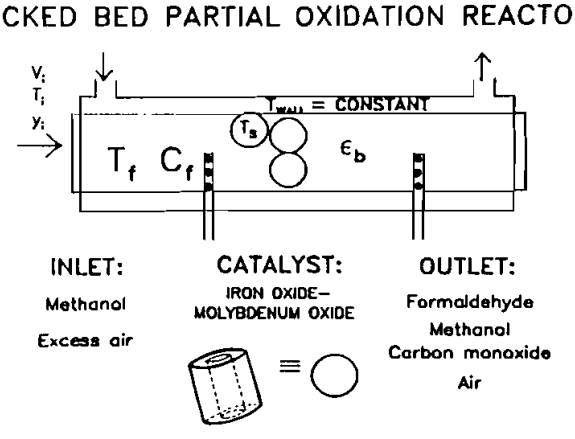


FIGURE 1 Schematic of packed bed reactor.

phase oxygen replaces the lattice oxygen. The two-step redox mechanism is:

1. methanol + oxidized catalyst $\xrightarrow{k_1}$ formaldehyde + reduced catalyst

2. reduced catalyst + oxygen $\xrightarrow{k_0}$ oxidized catalyst

Strong evidence for an oxidation-reduction mechanism is that small amounts of methanol can be oxidized in a pulse reactor without the presence of oxygen if the catalyst has been previously oxidized.

If the rates of these two reactions are equated and some algebraic manipulations performed, the rate of oxidation of methanol in terms of partial pressures of the reactants and surface-adsorbed species is:

$$R_M = \frac{k_1 p_M^m k_0 p_0^n}{N k_1 p_M^m + k_0 p_0^n}\left(\frac{1}{1+\sum_j K_j p_j}\right) \rightarrow \frac{k_1 p_M^m}{1+\left(\frac{N k_1}{k_0 p_0^n}\right)} p_M^m \tag{3}$$

Although numerous complex kinetic schemes may be formulated (for example, Jiru *et al.*, 1966), there is not sufficient data available to determine large numbers of constants. Thus, a simpler rate is not necessarily accurate mechanistically, but it can provide a good fit to data (Dente and Pasquon, 1965; Jiru, *et al.*, 1966; Pernicone *et al.*, 1969; Santacesaria *et al.*, 1981). A major simplifying assumption in the final form of Eq. (3) is that no products or reactants adsorb on the surface of the catalyst. Some studies have shown that water (Pernicone *et al.*, 1968), formaldehyde (Jiru, *et al.* 1966), and methanol (Bibin and Popov, 1969) are adsorbed and consequently limit the fraction of surface available for the redox reaction. The modified reaction rate is proportional to the available fraction of catalyst surface. However, only water adsorption has been considered in quantitative detail (Santacesaria *et al.*, 1981), and only runs with excess water in the feed required the adsorption term to adequately fit the data. Water adsorption is of importance only at low temperature below 240°C when the overall rate is small. Since our experiments did not include excess water in the feed, water adsorption was not considered in kinetic parameter identification.

There is disagreement in the literature concerning the correct values of the reaction order (the constants $m$ and $n$ in the rate expression). An overview of the literature indicates that the order with respect to oxygen is either 0 or $\frac{1}{2}$. Since oxygen is in large excess, the quantity $p_0^{1/2}$ is approximately constant so that the reaction order with respect to oxygen is not important to the overall rate, and the best approximation for $N/p_0^{1/2}$ was found to be unity. The order with respect to methanol is chosen by the values which give the best fit to data, and results of various studies have given orders of either $\frac{1}{2}$ or 1. Data from our reactor gave a considerably better fit for $m = \frac{1}{2}$.

Under these assumptions, the final rate expression for methanol oxidation is:

$$R_M = \frac{k_1 p_M^{1/2}}{1 + K_a p_M^{1/2}} \tag{4}$$

where

$$K_a = \left(\frac{Nk_1}{k_0 p_0^n}\right)$$

and the ratio of kinetic constants must be identified through experiment. Some authors have indicated that $k_1 \sim k_0$ (Dente *et al.*, 1964; Jiru *et al.*, 1966), and a recent study has fitted data to give values of both $k_1$ and $k_0$ (Santacesaria *et al.*, 1981). From our experimental studies, we have estimated values for the kinetic parameters $k_1$ and $K_a$ of Eq. (4), where

$$k_1 = A_1 \exp(-E_1/R_g T)$$
$$K_a = Nk_1/k_0 p_0^{1/2} = A_a \exp(-E_a/R_g T)$$

and these parameters are given in Table I.

The most important secondary reaction in the oxidation of methanol is the subsequent oxidation of formaldehyde to carbon monoxide and water. Few authors have presented a kinetic model for this reaction on this type of catalyst. The most extensive treatment considers diffusion within the catalyst pores and the reaction rate is assumed to be a power law expression in terms of the partial pressures of formaldehyde and oxygen within the interior of the catalyst (Dente

TABLE I

System parameters

| | | |
|---|---|---|
| A. Reactor | | |
| flow = 1.4*E*-3 Kg/s | $L = 0.7$ m | $r_t = 0.0133$ m |
| $G = 2.52$ Kg/m$^2$-s | $P_{\text{inlet}} = 1.55$ atm | $\varepsilon_b = 0.5$ |
| $Re = \sim 300$ | $P_{\text{outlet}} = 1.3$ atm | $\rho_b = 1000$ Kg/m$^3$ |
| $F = (GC_p)_f = 2400$ J/m$^2$-s-K | | |
| B. Catalyst | | |
| $\rho_s = 2000$ Kg/m$^3$ | order = 0.5 | $A_a = 27$ |
| $\varepsilon_p = 0.57$ | $A_1 = 6250$ | $E_a = 2000$ cal/mole |
| $d_c = 0.460$ cm | $A_2 = 5.6$ | tortuosity = 2 |
| $d_s = 0.537$ cm | $E_1 = 19000$ cal/mole | $D_e = 0.049$ cm$^2$/s @600K |
| $d_x = 0.284$ cm | $E_2 = 16000$ cal/mole | $S_v = 1050$ m$^2$/m$^3$ |
| $d_0 \times d_i \times l_p = 4.3 \times 1.7 \times 3.5$ mm | | |
| C. Dimensionless Parameters | | |
| $Bi_h = h_{fs} d_x/2\lambda = 1$; $Bi_m = k_m d_x/2D_e = 175$ | | |
| $Pe'_{sr} = Pe'_{sz} = F d_c/k_s = 50$ | | |
| $Pe_{sr} = Fr_t/k_s = 150$; $Pe_{sz} = FL/k_s = 8000$ | | |
| $Pe'_{hr} = F d_c/k_{er} = 8.6$; $Pe_{hr} = Fr_t/k_{er} = 25$ | | |
| $Pe'_{fr} = F d_c/k_{fr} = 10.4$; $Pe_{fr} = Fr_t/k_{fr} = 30$ | | |
| $Pe'_{hz} = F d_c/k_{ez} = 0.44$; $Pe_{hz} = FL/k_{ez} = 68$ | | |
| $Pe'_{fz} = F d_c/k_{fz} = 2.0$; $Pe_{fz} = FL/k_{fz} = 300$ | | |
| $Pe'_{mr} = v d_c/D_r = 6.6$; $Pe_{mr} = vr_t/D_r = 19$ | | |
| $Pe'_{mz} = v d_c/D_z = 2.0$; $Pe_{mz} = vL/D_z = 300$ | | |
| $Bi_{wf} = h_{wf} r_t/k_{fr} = 5.5$; $Bi_{ws} = h_{ws} r_t/k_s = 5.5$ | | |
| $Bi_w = h_w r_t/k_{er} = 5.5$. | | |
| $St_m = S_v L k_m/v = 74$; $St_h = S_v L h_{fs}/F = 90$ | | |
| $Le = (\rho C_p)_s/(\rho C_p)_f = 1350$ | | |

and Collina, 1965):

$$-R_{CO} = k_2 p_F^{m'} p_0^{n'} \tag{5}$$

However, our experiments indicate that a redox expression of the form of Eq. (3) gives a correct fit to data. By considering the selectivity of consecutive reactions (Wheeler, 1957), approximating surface concentrations by those in the gas phase, and using the value $n' = 0$ (because of large excess oxygen), the redox rate expression becomes:

$$-R_{CO} = \frac{k_2 p_F^{1/2}}{1 + p_F^{1/2}}; \tag{6a}$$

where the partial pressure of formaldehyde, $p_F$, may be calculated by difference as

$$p_F = (y_{M,i} - \eta_M y_{M,f} - y_{CO,f}) P_T \tag{6b}$$

An activation energy of 16 Kcal/mole was used to successfully represent experimental data (Schwedock, 1983).

## DYNAMIC REACTOR MODELS

Dynamic models are the basis for control studies and the examination of transient phenomena such as traveling waves and undamped oscillations. By contrast, steady state models have usually been used for reactor design, fitting kinetic data, and model verification or selection. Much early reactor modelling was limited to steady state reactor behavior, because addition of the time "dimension" caused considerable complications. However, accurate dynamic models are currently much more tractable due to improvements in numerical methods and computers. Earlier work on simulation of packed bed reactor dynamics and studies in which reactor experiments were compared with the mathematical model have been summarized elsewhere (Windes, 1986).

In the general case for spherical particles in a cylindrical reactor, the partial differential equations are written in terms of three space variables and time. They are:

Solid:

mass:
$$\varepsilon_p \frac{\partial c_s}{\partial t} = D_e \frac{1}{x^2} \frac{\partial}{\partial x}\left(x^2 \frac{\partial c_s}{\partial x}\right) - R'(c_s, T_s) \tag{7}$$

heat:
$$(1-\varepsilon_b)(\rho C_p)_s \frac{\partial T_s}{\partial t} = (1-\varepsilon_b)\lambda \frac{1}{x^2} \frac{\partial}{\partial x}\left(x^2 \frac{\partial T_s}{\partial x}\right) + k_{sz} \frac{\partial^2 T_s}{\partial z^2} + k_{sr} \frac{1}{r} \frac{\partial}{\partial r}\left(r \frac{\partial T_s}{\partial r}\right) + (1-\varepsilon_b)(-\Delta H) R'(c_s, T_s) \tag{8}$$

Fluid:

mass:
$$\varepsilon_b \frac{\partial c_f}{\partial t} = D_z \frac{\partial^2 c_f}{\partial z^2} + D_r \frac{1}{r}\frac{\partial}{\partial r}\left(r \frac{\partial c_f}{\partial r}\right) - \frac{\partial (c_f v)}{\partial z} + S_v k_m (c_u - c_f) \tag{9}$$

heat:
$$\varepsilon_b (\rho C_p)_f \frac{\partial T_f}{\partial t} = k_{fz} \frac{\partial^2 T_f}{\partial z^2} + k_{fr} \frac{1}{r}\frac{\partial}{\partial r}\left(r \frac{\partial T_f}{\partial r}\right) - \frac{\partial (v \rho C_p)_f}{\partial z} + S_v h_{fs} (T_u - T_f) \tag{10}$$

Some simplication of these equations is required before computation. Classification of the relevant equations for various types of mathematical models and a discussion of their development has been presented in several reviews (Amundson, 1970; Karanth and Hughes, 1974a; Froment, 1972; Hlavacek, 1970; Carberry, 1981) and in standard reaction engineering texts.

The wide range of mass and energy transport phenomena in the typical packed bed catalytic reactor is divided into three categories depending upon the size scale in which it occurs:

1. kinetics of adsorption and chemical reactions which take place within the pores of the solid catalyst;
2. mass and energy transport within the interior of the catalyst pellet and between the solid and fluid interface;
3. reactor scale heat transport in the solid and fluid phases, mass and momentum transport in the fluid phase.

In order to provide an efficient dynamic model acceptable for real-time computation it is desirable to separate these three categories and attack each one individually.

### *Modelling the Adsorption/Reaction Phenomena*

For this reaction system, it is known that the dynamics of adsorption and desorption are fast relative to the other time scales. Thus the quasi-steady state may be applied and overall kinetic rate expressions, Eqs. (4, 6), may be used.

### *Modelling the Single Catalyst Particle*

A separation of the single catalyst particle reaction-diffusion problem from the overall reactor model is an important simplification. This means that a quasi-steady state effectiveness factor can be calculated which is dependent only on the local reactor concentration and temperature. This separation is readily accomplished when

(i) the catalyst particle has no significant internal temperature gradients (isothermal particle)
(ii) the dynamics of gas phase diffusion in the catalyst particle are fast relative to

thermal transients (quasi-steady-state concentration profiles in the catalyst particle)

Both of these assumptions are valid for the present reaction system (and are usually valid in general). Note that only the main reaction (1) is subject to diffusion limitation; the secondary reaction (2) is relatively slow, does not rely on diffusion to supply its reactant, and is not strongly influenced by diffusion.

The resulting reaction-diffusion problem is considered separately off-line, and an effectiveness factor analysis has been developed to accurately incorporate these results into reactor simulation. Because of the complexity of the reaction rate expression, no analytical solution is available relating the effectiveness factor to the Thiele modulus. Various asymptotic and approximate results were investigated, but none gave results of the desired accuracy, especially in the case when the catalyst temperature rise was not known. Therefore, the mass and energy balance equations for the catalyst are solved numerically by orthogonal collocation to provide effectiveness factor charts for the catalyst.

The dimensionless equations for a single reaction (methanol oxidation) with one independent component (methanol) assuming constant effective thermal conductivity and constant effective diffusivity in a porous catalyst particle are:

$$\frac{\partial c}{\partial \tau_p} = \frac{1}{x^2}\frac{\partial}{\partial x}\left(x^2 \frac{\partial c}{\partial x}\right) - \phi^2(c_f', T_f')R(c, \theta) \tag{11}$$

$$Le_p \frac{\partial \theta}{\partial \tau_p} = \frac{1}{x^2}\frac{\partial}{\partial x}\left(x^2 \frac{\partial \theta}{\partial x}\right) + \beta\phi^2(c_f', T_f')R(c, \theta) \tag{12}$$

with boundary conditions at $x = 1$:

$$\frac{\partial c}{\partial x} = Bi_m(1 - c_u) \tag{13}$$

$$\frac{\partial \theta}{\partial x} = Bi_h(1 - T_u) \tag{14}$$

where the symbols are defined in the Nomenclature. The geometry of the Fe/Mo catalyst particle in the reactor is a Raschig ring—a cylinder with a hole along the axis. Since this geometry would be difficult in computations, the particle is considered to be an "equivalent" sphere with diameter which maintains the same volume to surface ratio. After making the simplifications of isothermal pellet and pseudo-steady state catalyst particle concentration profiles mentioned above, the catalyst particle equations become:

$$\frac{1}{x^2}\frac{\partial}{\partial x}\left(x^2 \frac{\partial c}{\partial x}\right) - \phi^2(c_f', T_f')R(c, T_u) = 0 \tag{15}$$

$$Bi_h(1 - T_u) + \beta\phi^2(c_f', T_f')E^2\int_0^1 Y(p_M)x^2\,dx = 0 \tag{16}$$

where $Y(p_M)$ is dimensionless partial pressure. The method of orthogonal

collocation applied to this this problem is discussed by several sources (Hansen, 1971; Finlayson, 1972, 1974; Villadsen and Michelsen, 1978).

The equations which must be solved numerically are:

$$\sum_{k=1}^{NP} B_{c,ik}c_k + q_i - \phi^2(c_f', T_f')E^2Y_i = 0, \qquad i = 1, NP \tag{17}$$

$$3Bi_h(1 - T_u) + \beta\phi^2(c_f', T_f')E^2 \sum_{k=1}^{NP} W_kY_k = 0 \tag{18}$$

The surface partial pressure $Y_{NP+1}$ has been eliminated by algebraic substitution of the collocated form of boundary condition (13), and the interpolation weights ($W_k$) modified accordingly. The boundary concentration ($c_u$) is an explicit function of the concentrations at the interior collocation points. From these equations the effectiveness factor, $\eta$, may be calculated as:

$$\eta = \frac{\bar{R}'}{R'(c_f', T_f')} = E^2 \sum_{k=1}^{NP} W_kY_k \tag{19}$$

The effectiveness factor cannot be expressed as a unique function of the Thiele modulus because of: (i) the complex redox kinetics expression for the dependence of rate upon partial pressure, (ii) the temperature rise in the external boundary layer of the pellet. Instead, the effectiveness factor is given as a two-dimensional mapping as a function of two of the three parameters [$\phi$, $T'$, $p_{Mf}$]. Alternatively, some other quantity $\hat{\phi}$ could be used which would collapse all curves to $\eta = f(\hat{\phi})$. However, in our work we found that $\eta = \eta(\phi, p_M)$ worked quite well. To illustrate, Figure 2 shows plots of the effectiveness factor versus Thiele modulus at constant partial pressure in the fluid. A lower bound of effectiveness factor occurs as $p_M$ becomes small. In addition, the effectiveness factor is found to be a linear function of partial pressure at constant Thiele modulus. Thus, knowing the

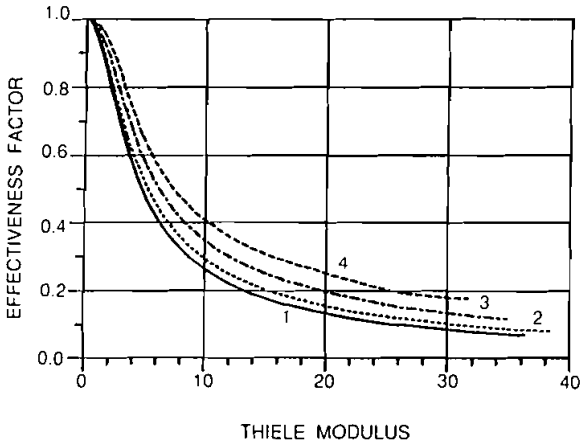


FIGURE 2 Effectiveness factor versus Thiele modulus. Based on fluid conditions. Lines represent 4 different methanol gas phase partial pressures (atm). (1) —— 0.002; (2) · · · · 0.02; (3) · – · – 0.04; (4) – – – 0.06.

effectiveness factor, $\eta$, as a function of Thiele modulus $\phi$, at two separate partial pressures allows calculation of $\eta$ for all fluid phase temperature and methanol concentrations.

The procedure is efficiently accomplished by the following steps:

1. At a low value of bulk gas partial pressure $p_{M^*}$ (curve 1 of Figure 2) an empirical formula $\eta^* = f(\phi)$ is needed. However, $f(\phi)$ is a high order polynomial, and a functional form suggested by an analytical solution for the effectiveness factor in an ideal case is more efficient. $\eta^*$ is represented in terms of a modified Thiele modulus $\phi^*$ using the solution for a first order reaction in an isothermal spherical pellet:

$$\eta^* = \frac{3}{(\phi^*)^2}[\phi^* \coth \phi^* - 1] \tag{20}$$

The modified Thiele modulus $\phi^*$, introduced to account for deviations from the ideal first order case in Eq. (20), is defined to be a polymial function of the actual Thiele modulus:

$$\phi^* = P_1 + P_2\phi + P_3\phi^2 + P_4/\phi \tag{21}$$

The constants are determined to minimize the least squares error between $\eta^*$ predicted by Eq. (20) and the numerical collocation solution for $\eta$ vs. $\phi$ at $p_{M^*}$ computed by Eqs. (17–19).

2. The influence of changes in bulk gas phase methanol partial pressures, $p_M$, upon the effectiveness factor can be found for the relevant range of $p_M$ values $p_{M^*} \leq p_M \leq p_M^*$ by the empirical formula:

$$\eta = \eta^* + D^*(p_M - p_{M^*})/(p_M^* - p_{M^*}) \tag{22}$$

Here the parameter $D^*$ is the rate of change $\eta$ vs. $P_M$ and is a function of $\phi$. $D^*$ is determined by computing $\eta$ numerically using Eqs. (17–19) at $P_M^*$ (high partial pressure), and then solving Eq. (22) for $D^*$. By repeating this calculation at several values of Thiele modulus and constant $P_M^*$, $D^*$ can be correlated as a closed-form function of $\phi$ from the regression equation

$$D^* = D_1 + D_2\phi + D_3 \exp(D_4\phi) + D_5/\phi \tag{23}$$

where the parameters, $D_i$, $i = 1, \ldots, 5$, are found from a least squares fit of Eqs. (22, 23) to the numerical collocation solution (17–19) for $\eta$.

This method is dependent upon the observation that the effectiveness factor is effectively linear in partial pressure at constant Thiele modulus, but is found to be a good method for obtaining a rapidly computable form relating reactor conditions to the observed reaction rate when intrinsic kinetic parameters are known.

## THE PACKED BED REACTOR MODEL

Incorporating the effective reaction rate expression into the general model gives the following dimensionless equations for methanol, carbon monoxide, fluid

temperature, and solid temperature:

mass (species $j$):

$$0 = \frac{1}{Pe_{mz}}\frac{\partial^2 y_j}{\partial z^2} + \frac{a}{Pe_{mr}}\frac{1}{r}\frac{\partial}{\partial r}\left(r\frac{\partial y_j}{\partial r}\right) - \frac{\partial y_j}{\partial z} - (1-\varepsilon_b)Da\bar{R}_j(p_j, T_s) \tag{24}$$

energy (fluid):

$$0 = \frac{1}{Pe_{fz}}\frac{\partial^2 T_f}{\partial z^2} + \frac{a}{Pe_{fr}}\frac{1}{r}\frac{\partial}{\partial r}\left(r\frac{\partial T_f}{\partial r}\right) - \frac{\partial T_f}{\partial z} + St_h(T_s - T_f) \tag{25}$$

energy (solid):

$$Le\frac{\partial T_s}{\partial \tau_r} = \frac{1}{Pe_{sz}}\frac{\partial^2 T_s}{\partial z^2} + \frac{a}{Pe_{sr}}\frac{1}{r}\frac{\partial}{\partial r}\left(r\frac{\partial T_s}{\partial r}\right) - St_h(T_f - T_s) + (1-\varepsilon_b)B_R\bar{R}_e \tag{26}$$

Boundary conditions:

$$r = 1 \qquad \frac{\partial T_f}{\partial r} = Bi_{wf}(T_w - T_f) \tag{27a}$$

$$\frac{\partial T_s}{\partial r} = Bi_{ws}(T_w - T_s) \tag{27b}$$

$$z = 0 \qquad \frac{\partial y}{\partial z} = Pe_{mz}(y - y_i) \tag{28a}$$

$$\frac{\partial T_f}{\partial z} = Pe_{fz}\tfrac{1}{2}(1+\sigma)(T_f - T_i) = \psi_0(T_f - T_i) \tag{28b}$$

$$\frac{\partial T_s}{\partial z} = \mu_0(T_s - T_i) \tag{28c}$$

$$z = 1 \qquad \frac{\partial y}{\partial z} = 0 \tag{29a}$$

$$\frac{\partial T_f}{\partial z} = Pe_{fz}\tfrac{1}{2}(1-\sigma)(T_f - T_w) = \psi_1(T_f - T_w) \tag{29b}$$

$$\frac{\partial T_s}{\partial z} = \mu_1(T_s - T_{ex}) \tag{29c}$$

where $\sigma$ and $\mu_0$ are parameters accounting for radial transport at the inlet and exit (which is similar to the approach of Young and Finlayson, 1973)

$$\sigma = \left[1 + \frac{24Bi_{wf}a}{Pe_{fr}Pe_{fz}(Bi_{wf}+3)}\right]^{1/2} \tag{30}$$

$$\mu_0 = Pe_{sz}\left[\frac{6Bi_{ws}a}{Pe_{sr}Pe_{sz}(Bi_{ws}+3)}\right]^{1/2}; \qquad \mu_1 = 0 \tag{31}$$

and the dimensionless quantities are defined by

$$\tau_r = \frac{tv_0}{L} \qquad c_j = \frac{c_j'}{c_{M_0}} \qquad y_j = \frac{y_j'}{y_{M_0}} \qquad T_s = \frac{T_s'}{T_0} \qquad T_f = \frac{T_f'}{T_0}$$

$$z = \frac{z'}{L} \qquad r = \frac{r'}{r_t} \qquad a = \frac{L}{r_t} \qquad Pe_{mz} = \frac{v_0 L}{D_z} \qquad Pe_{mr} = \frac{v_0 r_t}{D_r}$$

$$Pe_{fz} = \frac{\rho_f C_{pf} v L}{k_{fz}} = \frac{GC_{pf} L}{k_{fz}} \qquad Pe_{fr} = \frac{GC_{pf} r_t}{k_{fr}} \qquad Bi_{wf} = \frac{h_{wf} r_t}{k_{fr}}$$

$$Pe_{sz} = \frac{GC_{pf} L}{k_{sz}} \qquad Pe_{sr} = \frac{GC_{pf} r_t}{k_{sr}} \qquad Bi_{ws} = \frac{h_{ws} r_t}{k_{sr}} \tag{32}$$

$$\bar{R}_j = \frac{\eta_j R_j(p_j, T_s')}{\eta_0 R_M(p_0, T_0)} \qquad \bar{R}_e = \bar{R}_M + (-\Delta H_{CO}/-\Delta H_M)\bar{R}_{CO}$$

$$B_R = \frac{(-\Delta H_M)\eta_0 R_M(p_0, T_0) L}{GC_{pf} T_0} \qquad Da = \frac{\eta_0 R_M(p_0, T_0) L}{c_0 v_0} = \frac{\eta_0 R_M(p_0, T_0) L \bar{M}_w}{G_0}$$

$$St_h = \frac{S_v h_{fs} L}{GC_{pf}} \qquad Le = \frac{(1-\varepsilon_b)(\rho C_p)_s v_0}{(\rho C_p v)_f} = \frac{(1-\varepsilon_b)(\rho C_p)_s}{\rho_{f_0} C_{pf}}$$

Note that all equations involving the fluid phase are considered to be at pseudo-steady state, since the thermal time constant of the solid is approximately 1500 times greater than the fluid time constants. A commonly used simplification is to consider the entire reactor as a continuum with appropriately averaged properties. This results in a one phase or pseudohomogeneous model, which contrasts to the two phase or heterogeneous model described above. The pseudohomogeneous model has advantages that (i) only one temperature equation must be solved, and (ii) the parameters for the heat transfer properties of the solid and fluid which are difficult to identify separately in the heterogeneous model are more conveniently lumped into overall properties in a one phase model.

To compare the one and two phase models one must:

1. match the heat transfer parameters so that effective heat transfer is equivalent (Dixon and Cresswell, 1979),
2. use the appropriate effectiveness factor functions, either one based on the solid phase temperature for the heterogeneous model, or one for the pseudohomogeneous model based on the fluid temperature with a built-in steady state catalyst temperature rise.

Both the one and two phase models may be either one or two dimensional depending upon whether or not radial gradients are considered. Also, axial conduction and dispersion terms may either be considered or omitted. Consideration of all these possibilities gives a hierarchy of models as shown in Figure 3. Determination of the appropriateness of these models depends upon comparison by simulation, comparison with experimental results, and/or *a priori* selection and evaluation of parameter values.

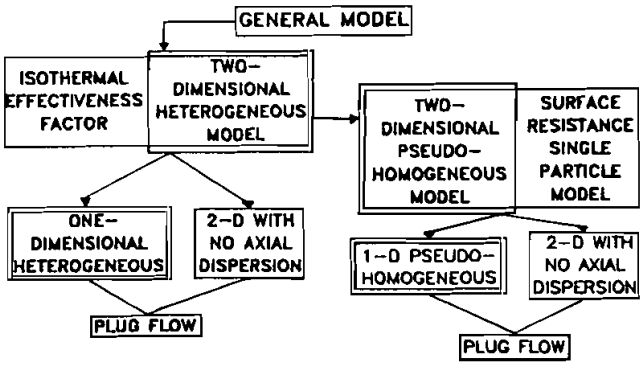


FIGURE 3 Hierarchy of reactor models.

## PARAMETER SELECTION

There are far too many parameters influencing a packed bed catalytic reactor to allow completely empirical parameter estimation. Values of some parameters must be selected through correlations found in the literature. *A priori* estimation of all the reactor parameters has been carried out in order to:

1. determine which important parameters could not be easily estimated and had to be determined experimentally,
2. provide a qualitative prediction of the reactor behavior before construction was completed,
3. assess the feasibility of eliminating experimental work at the design stage through *a priori* computer simulation.

The first two of these goals were accomplished, and the simulation provided excellent qualitative prediction of reactor performance. However, the uncertainty of crucial parameters such as kinetic rate constants and radial heat transport made precise *a priori* simulation impossible in this case. Some experimental identification of parameters was necessary to supplement those obtained from correlations. It appears that at least one experimental stage in scale-up is still required for good quantitative model development. Since the introduction of powerful numerical tools such as orthogonal collocation for solving this type of non-linear boundary value problem, the problem of obtaining accurate parameter values (rather than the task of solving the equations with speed and accuracy) is the limiting factor in improvement of packed bed reactor models.

The model parameters can be divided into four categories:

1. Kinetic parameters as discussed in a previous section.
2. Heat and mass transfer in the catalyst particle–conductivity, diffusivity, and interphase transfer. These parameters are estimated through correlations found in the literature.
3. Heat and mass transfer in the packed bed reactor: a) conductivity and diffusivity in the radial and axial direction in the solid and fluid phases, and b)

heat transfer at the wall of the reactor. Radial heat transfer and wall heat transfer have been estimated experimentally.

4. Dynamic parameters involving characteristic times for various processes. The ratio of solid to fluid thermal capacitance determines the rate of change of the temperature.

A listing of the various parameter values used in simulation is given in Table I, important correlations are listed in Appendix A, and a detailed discussion of how these parameters may be estimated is provided by Windes (1986).

Mass transfer occurs through mixing of the fluid elements since molecular diffusion has a negligible effect. Heat transfer includes conduction in the solid phase and conduction and dispersion in the fluid phase. The heat transfer is often expressed in terms of a stagnant thermal conductivity and a dynamic, flow dependent contribution which is due to fluid mixing effects. Although this partitioning is convenient experimentally, the individual components related to each phase must be determined for use in a heterogeneous model.

*Radial and axial solid phase conductivity* Since the catalyst is randomly packed, the bed of pellets is assumed to have the same conductivity in the radial and axial directions. This parameter is independent of flow. The most extensive treatment and the only consideration of hollow cylinders has been the geometric model of Schlunder and co-workers (Schlunder, 1978; Bauer and Schlunder, 1978b). The solid phase conductivity depends upon the conductivity of each pellet, radiation, pressure, area of surface contact, particle shape, and influence of the wall. After considering several additional correlations (e.g., DeWasch and Froment, 1972) the effective solid conductivity was taken to be approximately five to six times the molecular conductivity of the gas, yielding a solid Peclet number $Pe_s'$ of 50.

*Fluid phase radial thermal conductivity* For reactors cooled at the wall, the radial thermal conductivity is one of the most important parameters, and the majority of radial heat transfer takes place in the fluid phase. The mechanisms for fluid phase heat transfer are the molecular conductivity of the gas, radiation between voids, and dispersion of thermal energy due to the mixing of fluid elements. The most detailed model of these phenomena correlates experimental data with particle shape and reactor/particle diameter ratio (Bauer and Schlunder, 1978a). Hollow cylinders give a large improvement in radial mixing and long cylinders with thin walls are the most effective, with observed improvements of as much as 1000%. However, the packed bed in this study exhibited lower radial heat transfer than predicted by the correlations of Bauer and Schlunder.

*Effective radial thermal conductivity* The effective radial thermal conductivity is given as a combination of static and dynamic contributions or as the sum of the solid and fluid effective conductivities. These components have been calculated in the previous two sections, and the overall value can be obtained by addition of the reciprocal Peclet numbers (Kulkarni and Doriaswamy, 1980;

Schlunder, 1978).

$$\frac{1}{Pe'_{hr}} = \frac{1}{Pe'_{fr}} + \frac{1}{Pe'_{sr}} \tag{33}$$

A more detailed representation includes the interphase heat transfer and the heat transfer between the fluid and the wall (Dixon and Cresswell, 1979):

$$1/Pe_{hr} = 1/Pe_{fr} + (1/Pe_{sr})\frac{(Bi_{wf}+4)/Bi_{wf}}{8/N_s + (Bi_{ws}+4)/Bi_{ws}} \tag{34}$$

More detailed expressions which include heat of reaction effects have been developed (Windes, 1986); however, these additional terms do not have a significant effect on the overall Peclet number for the operating conditions of our study.

*Heat transfer to reactor wall* For a heterogeneous reactor model, the heat transfer to the wall must be partitioned between fluid and solid phases. An overall wall heat transfer coefficient is sufficient for the pseudohomogeneous model. A detailed series-parallel mechanism has been used for several years (Yagi and Kunii, 1960), but experiments have shown a large amount of scatter in the results. Experiments estimating wall heat transfer from wall mass transfer (Olbrich and Potter, 1972) indicated a wall heat transfer coefficient much higher than that found in other experiments. Various forms for correlating the wall heat transfer in terms of a Nusselt number are compared and discussed in Li and Finlayson (1977). A few authors have correlated the heat transfer coefficient in terms of the Biot number (Dixon *et al.*, 1978).

There are almost no published data on the solid/wall heat transfer coefficient. An estimate obtained from the series-parallel model neglecting all fluid phase terms indicates a Biot number $Bi_{ws}$ of ~6. Due to the large uncertainty of the correlations for the wall heat transfer coefficient, this parameter was estimated from experiments without reaction (Schwedock, 1983). These experiments indicate a larger amount of wall heat transfer than predicted by Dixon's correlation. For the heterogeneous model, the $Bi_{ws}$ and $Bi_{wf}$ were set to the same value since we had no method of separately identifying them.

*Effective axial thermal conductivity* The axial Peclet number ($Pe'_{hz}$) includes stagnant and flow dependent components. In using and comparing one and two phase models, an equivalence relationship is needed between the effective conductivity of the pseudohomogeneous model and the parameters of axial conductivity in the heterogeneous model. Two different equivalence relationships have been proposed (Vortmeyer and Schaeffer, 1974; Dixon and Cresswell, 1979), compared, and discussed (Vortmeyer and Berninger, 1982; Cresswell and Dixon, 1982). Since experimental data indicate that $Pe'_{hz}$ is substantially less than the asymptotic value of $Pe'_{mz} = 2$ at high flow rates (Votruba *et al.*, 1972; Gunn and Desouza, 1974), inclusion of the interphase heat transfer in the effective axial conductivity (Vortmeyer and coworkers) seems justified. Cresswell and Dixon

modified the equivalence relation to include wall-cooled reactors:

$$\frac{1}{Pe'_{hz}} = \frac{1}{Pe'_{fz}}\left[1 + \frac{64}{Pe_{hr}}\left(\frac{Bi_w}{Bi_w + 4}\right)\left(\frac{d_p}{d_t}\right)\right] + \frac{1}{Pe'_{sz}} + \frac{1}{St'_h} \tag{35}$$

For our reactor system, this expression gives $Pe'_{hz} = 0.44$. Using this value (as opposed to neglecting axial heat transfer) has little effect on conversion and affects the temperature profile by no more than 5 C.

## SOLUTION OF THE REACTOR MODEL

The previous sections have laid the foundation for executing an efficient simulation of the packed bed methanol oxidation reactor. As commonly done in reactor modelling, the partial differential equations were converted to ordinary differential equations and algebraic equations by the method of orthogonal collocation (Villadsen and Stewart, 1967; Finlayson, 1971, 1974; Young and Finlayson, 1973; Villadsen and Michelsen, 1978). The collocation was done in the radial and axial directions, and computations for collocation points and weights were executed by subroutines given by Villadsen and Michelsen (1978). The final equations consisted of one set of non-linear ODE's for solid temperature to be integrated in time, a linear set of algebraic equations for fluid temperature, and two sets of non-linear algebraic equations for two independent reaction species, methanol and carbon monoxide. The algebraic equations were solved at each step in time. The number of equations in each set was equal to the number of interior collocation points, since the boundary collocation points were eliminated in terms of the interior points. The final collocation equations for the heterogeneous model are shown in Appendix C.

As indicated above in Eqs. (28–31), the fluid phase equations include the classical axial boundary conditions used for the pseudohomogeneous model, except that these boundary conditions are modified to account for the two dimensional nature of the problem (Young and Finlayson, 1973). The inclusion of radial heat transfer in the axial boundary conditions (28b) results in decreased heat losses from the entrance end of the reactor. The 2-D boundary condition effectively alters the axial Peclet number by ~10–15%. However, the resultant change in temperature profiles, conversion, and selectivity is insignificant.

Nontrivial solid phase axial boundary conditions have been derived for the two dimensional heterogeneous model. The boundary conditions (28c, 29c) are based on the method used by Young and Finlayson (1973) without fluid flow terms. A one-point collocation solution is applied to axial conduction in a solid cylinder, and the solid phase heat flux at the exit is assumed to be zero.

After application of the orthogonal collocation method to a particular type of reactor model, three numerical factors which determined the speed of solution for a particular transient simulation were the solution method, error criteria, and number of collocation points. A standard polyalgorithmic package "EPISODE" (Byrne and Hindmarsh, 1975) was used to integrate the equations in time. A

variable step-size, variable order Adams method, with functional iteration suitable for non-stiff problems was satisfactory and was faster than other options. The slow step in the solution procedure is repeatedly solving the nonlinear algebraic equations at each time derivative evaluation. A successive substitution method using an initial guess matching the solution of the previous time step and a "damping parameter" to achieve convergence proved to be the most effective method. An alternative method with a user-written Newton's method used substantially fewer iterations and had better convergence properties, but it was 30–50% slower due to Jacobian evaluations. A standard non-linear equation package was an order of magnitude slower still.

Convergence of the temperature and concentration profiles was observed as the number of collocation points increased; however, the number of collocation points is critical in adjusting the speed of the simulation. The most important difference is in changing from one to two radial collocation points. Two radial points takes three to four times as long to solve as one radial point, but significant differences in the results occur due to the steep radial temperature profiles and the highly nonlinear reaction rate. Three radial collocation points give only a slight improvement over two while taking at least three times as much computer time; therefore, two radial collocation points is the recommended choice. Solutions with six axial collocation points often show numerical artifacts for steep profiles, and fewer axial points give inaccurate results. Ten axial points give accurate results for all stable cases modelled for this reactor, but eight axial points appear to be sufficient for experimentally realistic operating conditions. In general, the number of collocation points required to represent a converged solution will depend upon the steepness of the profiles and the adequacy of profile representation by polynomials. The axial profiles of the methanol oxidation reactor are moderate, otherwise more complicated collocation schemes would be necessary.

## COMPARISON WITH EXPERIMENTAL DATA

The realism and validity of a mathematical model can best be evaluated by comparing simulations with experimental data. The reactor model has been compared with other work dealing with methanol oxidation in a packed bed reactor. In Figure 4, the circular points represent the pilot plant reactor data for one set of experimental conditions (Emig *et al.*, 1972; Panthel, 1977). The solid lines represent calculations made using literature correlation parameters with only the kinetic pre-exponential factor adjusted to account for the unknown catalyst activity. The hot spot occurred too close to the entrance of the reactor, and the temperature decreased too rapidly downstream of the hot spot. However, Panthel and Emig *et al.* fit all of their data using a much lower wall heat transfer coefficient than is given by published correlations. If the Biot number at the wall is reduced by a factor of two, then a good match is obtained with the results of Panthel for three different experimental conditions, and the dotted line in Figure 4 shows one such case.

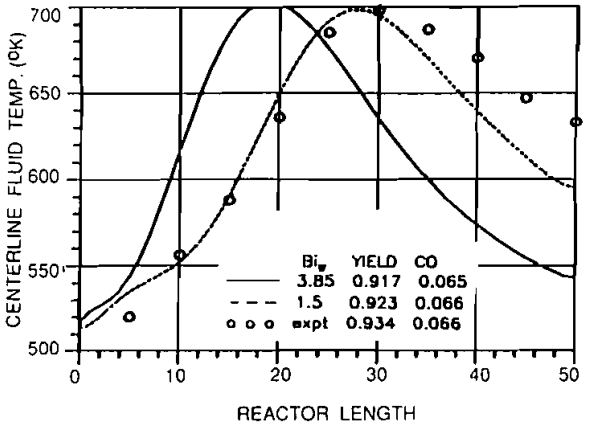


FIGURE 4 Comparison between simulation and experiment. $T_i = T_w = 513°K$, $y_{1i} = 0.05$. Data from Panthel (1977).

The second example is from work done in Italy in the 60's and early 70's (Dente *et al.*, 1966; Dente *et al.*, 1972). Figure 5 shows that good agreement is obtained between our model and their experiments by adjusting only the pre-exponential kinetic parameter. Half order dependence on methanol partial pressure as indicated by their experiments gives better results than a first order dependence as suggested by some later literature. The later paper of Dente showed reactor modelling which predicted excessive hot spot temperatures for a feed mole fraction of 0.07. Our simulations also gave hotter temperature profiles than the experimental data.

Results comparing model to experiment for our methanol oxidation reactor are presented in the sequel.

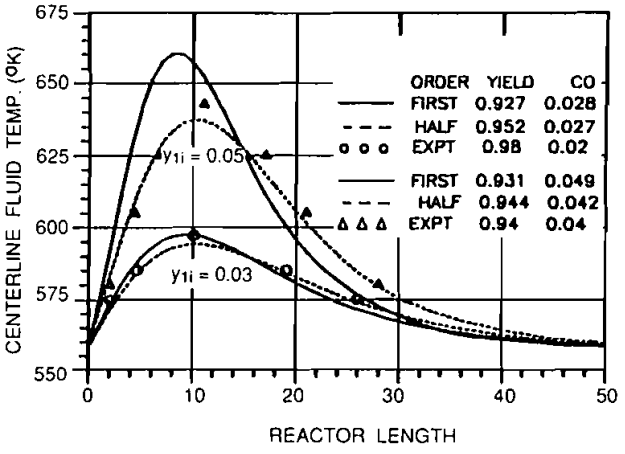


FIGURE 5 Comparison between simulation and experiment. $T_i = T_w = 555°K$, $y_{1i} = 0.03$, 0.05. Data from Dente *et al.* (1972).

## STEADY STATE SIMULATION RESULTS

Having established that the model can successfully represent experimental data from a variety of laboratories, it is useful to study the effect of operating conditions and reactor parameters on reactor behavior.

Sensitivity of the model to kinetic, transport, and operating parameters has been assessed by steady state simulation. Strong interactions exist between many of these parameters, and the sensitivity depends on the set of values chosen for the standard steady state about which the parameters are varied. Here the base case parameter set was selected to match the experimental results from our reactor.

### *Parametric Sensitivity*

Figure 6 shows steady states for different values of the kinetic pre-exponential factor (i.e., catalyst activity) for the primary reaction. As the rate increases, the hot spot shifts toward the entrance of the reactor. The temperature increase is limited for fast reaction rates because of depletion of the methanol in the inlet region of the reactor. The chief factor in limiting the parametic sensitivity to kinetic parameters is the significant diffusion limitation within the catalyst. If the effectiveness factor is taken to be unity, the reactor exhibits runaway behavior with small variations in the reaction rate parameters. However, in reality, diffusion limitations are significant and changes in the effective diffusivity within the catalyst pores has a large effect near the reactor hot spot (cf. Figure 7).

Radial Peclet number and wall Biot number have similiar effects on reactor performance and are the most important heat transfer parameters. Reactor

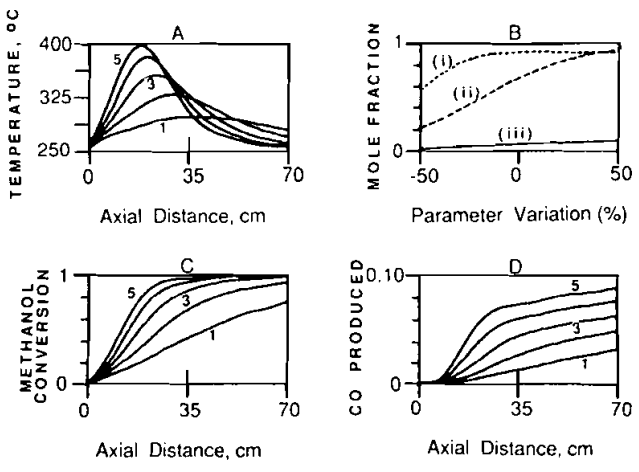


FIGURE 6 Steady state parametric sensitivity to kinetic pre-exponential factor. (1) −40%; (2) −20%; (3) base case, 0%; (4) +20%; (5) +40%. A: Centerline axial temperature profiles; B: Performance with parameter variation: (i) Yield, (ii) Conversion @ 25 cm, and (iii) CO production; C: Axial methanol conversion profile; D: Axial profile of mole fraction carbon monoxide production.

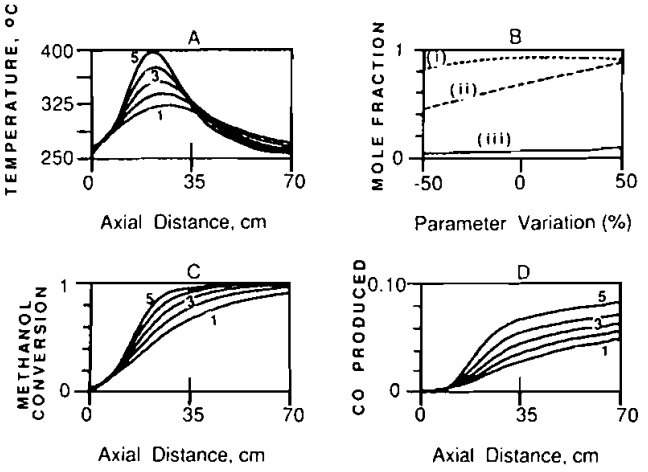


FIGURE 7 Steady state parametric sensitivity to effective diffusivity in the catalyst. (1) −40%; (2) −20%; (3) base case, 0%; (4) +20%; (5)+40%. A: Centerline axial temperature profiles; B: Performance with parameter variation: (i) yield, (ii) conversion @ 25 cm, and (iii) CO production; C: Axial methanol conversion profile; D: Axial profile of mole fraction carbon monoxide production.

temperature and composition profiles are shown in Figure 8 for changing values of radial Peclet number. Due to the large radial temperature gradients of up to 80°C over a distance of 1.3 cm, the radial Peclet number is the most important heat transfer parameter. The majority of the radial heat transfer takes place by mixing in the gas, and varying the effective radial thermal conductivity by 20% can change the hot spot temperature by 40°C. Since this reactor exhibits a large wall heat transfer coefficient, the sensitivity to the Biot number is considerably less

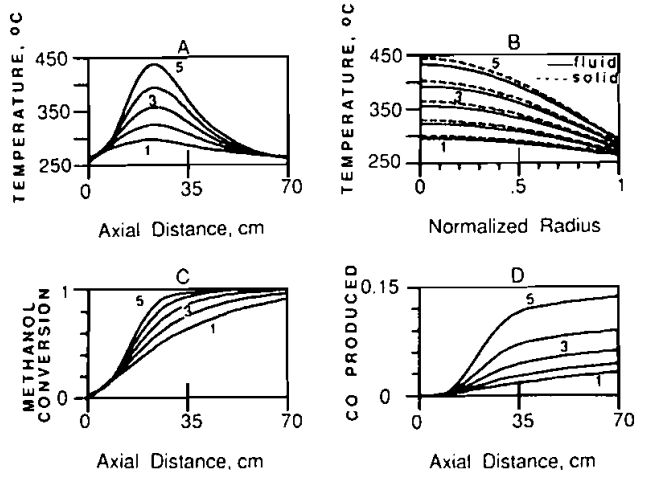


FIGURE 8 Steady state parametric sensitivity to radial fluid Peclet number–$Pe_{fr}$. (1) −40%; (2) −20%; (3) base case, 0%; (4) +20%; (5) +40%. A: Centerline axial temperature profiles; B: Radial temperature profile at 25 cm; C: Axial methanol conversion profile; D: Axial profile of mole fraction carbon monoxide production.

than for radial Peclet number. Thus, heat transfer within the bed rather than at the wall is limiting. The particle/fluid heat transfer coefficient has been estimated by correlations, and the reactor was found to be operating in a region of parametric insensitivity where a large increase in fluid-particle heat transfer causes little change in reactor performance. However, the reactor is highly sensitive if $h_{fs}$ is decreased below ~50% of the base value. Sizeable variations in radial or axial mass dispersion caused little change in the modelling results and the compositions are predicted to be approximately uniform over the reactor radius.

*Operating Conditions*

The effect different operating conditions have on the two-dimensional heterogeneous model is shown in Figures 9–11. Each of the operating variables—wall temperature, feed temperature, feed mole fraction, and feed flow rate—have a value for which the yield is maximized. The carbon monoxide production changes nonlinearly as a function of the operating variables. Increasing the feed temperature (Figure 9) shifts the hot spot toward the entrance and increases the temperature in the first portion of the reactor; however, this causes a decrease in temperature in the latter half of the reactor. Increases in wall temperature (Figure 10) or feed mole fraction cause the temperatures throughout the reactor to rise with the greatest effect at the hot spot. The position of the hot spot shifts only a small amount. Increasing the flow rate through the reactor shifts the hot spot toward the exit and makes the hot spot less severe (Figure 11).

The effect of reactor operating conditions are compared for four different model types (Figures 12–14), and the model equations for each model type are listed in Appendix B. The different models show qualitatively similar yield

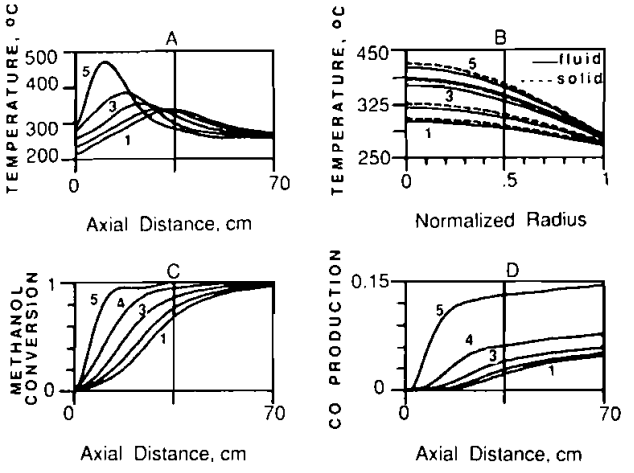


FIGURE 9 Steady state profiles for variations in feed temperature. $T_i$ = (1) 200, (2) 220, (3) 240, (4) 260, (5) 280. A: Centerline axial temperature profiles; B: Radial temperature profile at 15 cm; C: Axial methanol conversion profile: D: Axial profile of mole fraction carbon monoxide production.

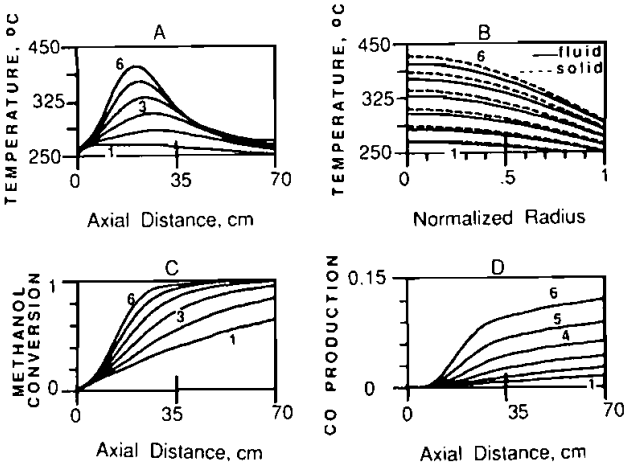


FIGURE 10 Steady state profiles for variations in wall temperature. $T_w$ = (1) 230, (2) 238, (3) 246, (4) 254, (5) 262, (6) 270. A: Centerline axial temperature profiles; B: Radial temperature profile at 25 cm; C: Axial methanol conversion profie; D: Axial profile of mole fraction carbon monoxide production.

curves, but the position of the optimal yield for the operating variables is different for the one and two dimensional models. Some trends are noted which give insight into the differences between models.

On the low temperature side of the optimal yield operating point, the feed flow rate and the wall tempeature have a dominant influence (cf. Figure 12). Feed temperatures (Figure 13) under 250°C and feed mole fractions (Figure 14) less than 0.05 have only a small effect on product yield. By contrast, at high feed

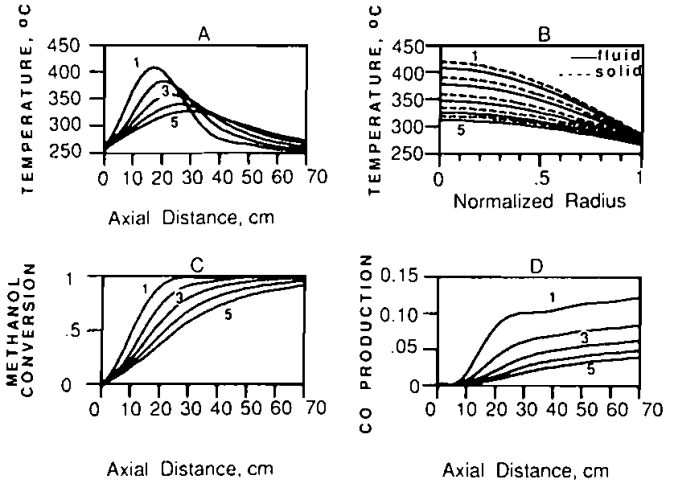


FIGURE 11 Steady state profiles for variations in feed flowrate (g/sec). $m$ = (1) 1.0, (2) 1.2, (3) 1.4, (4) 1.6, (5) 1.8. A: Centerline axial temperature profiles; B: Radial temperature profile at 17.5 cm; C: Axial methanol conversion profile; D: Axial profile of mole fraction carbon monoxide production.

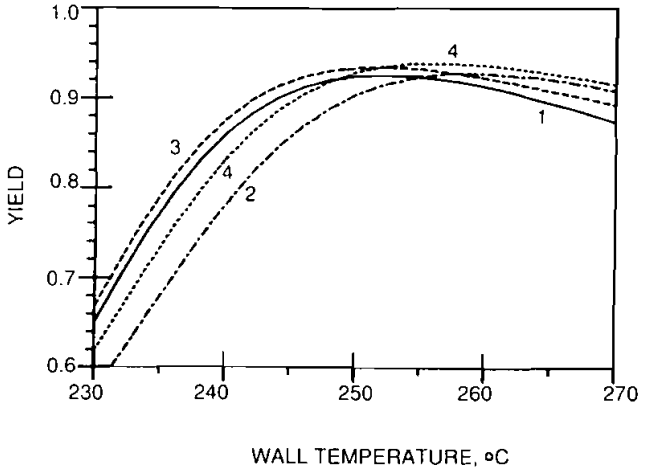


FIGURE 12 Formaldehyde yield with varying wall temperature—model comparison. (1) —— 2-D heterogeneous; (2) · – · – 1-D heterogeneous; (3) – – – 2-D pseudohomogeneous; (4) · · · · 1-D pseudohomogeneous.

temperatures and feed mole fraction methanol, the reactor is quite sensitive and approaches runaway conditions.

Figure 14 shows a distinctive local minimum in yield at ~3% methanol feed. This minimum is seen in simulations with all models and was also observed experimentally. It is not a characteristic of the model choice but results from the half-order redox kinetic expression. First-order redox kinetics do not show this type of behavior.

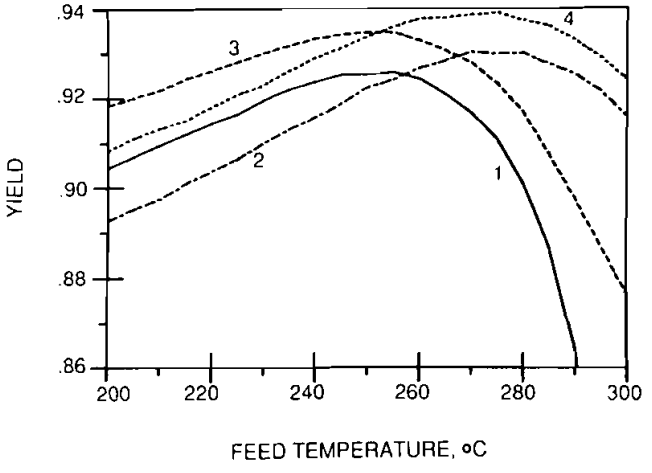


FIGURE 13 Formaldehyde yield with varying feed temperature—model comparison. (1) —— 2-D heterogeneous; (2) · · · – 1-D heterogeneous; (3) – – – 2-D pseudohomogeneous; (4) · · · 1-D pseudohomogeneous.

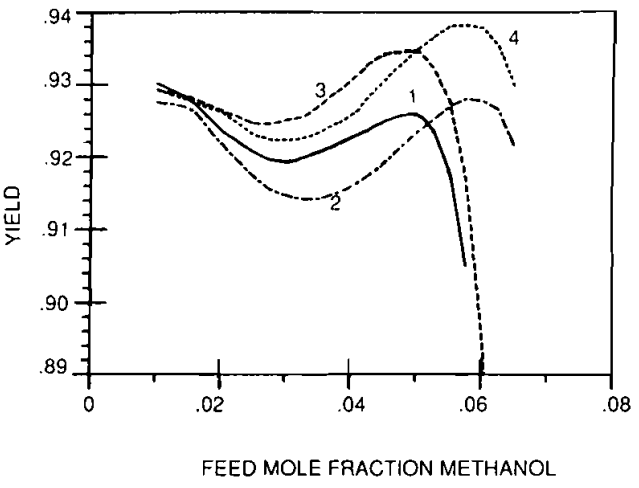


FIGURE 14 Formaldehyde yield with varying feed mole fraction—model comparison. (1) —— 2-D heterogeneous; (2) · – · – 1-D heterogeneous; (3) – – – – 2-D pseudohomogeneous; (4) · · · · 1-D pseudohomogeneous.

*Model Comparison*

In choosing between different models for a packed bed reactor with large radial temperature gradients operating at a stable steady state, we consider both one and two dimensional models and pseudohomogeneous and heterogeneous models. Some factors neglected in going from a two dimensional to a one dimensional model (as discussed by Pereira Duarte *et al.*, 1984b) are a non-parabolic radial temperature profile, axially varying overall heat transfer resistance, and the fact that interphase heat transfer causes interactions between solid and fluid phase heat transfer. However, the primary difference between the one and two dimensional representation is due to the nonlinear temperature sensitivity of the reaction rate. The radial mean temperature used in the one dimensional model indicates a lower rate of reaction and higher selectivity than the mean rate calculated from the multiple temperatures at radial collocation points in the two dimensional model. Thus a two dimensional model gives a better representation of the high temperature regions, more rapid reaction rates and greater by-product formation at the severe conditions near the center of the reactor. Use of a two dimensional model is most crucial when severe conditions exist in the reactor and the apparent activation energy is large, giving strong reaction rate dependence upon temperature. A reactor design based on a one dimensional model has a larger diameter and is longer than one based on a two dimensional model.

For the methanol oxidation reactor in this case study, severe conditions exist when the reactor operates near the optimum yield point. As can be seen from Figures 12–14, when the reactor operates at low temperatures (below the optimum yield point), the two dimensional model will give higher yields than the one dimensional model due to the larger average conversion rate of methanol to formaldehyde. When the reactor operates at temperatures above the optimum

yield point, the production of the by-product carbon monoxide gains importance, and the two dimensional model indicates lower yields than the one dimensional model. As a result, the two dimensional model predicts a lower optimum value for wall temperature, feed temperature, and feed mole fraction methanol, and a larger optimal flow rate.

The other major model assumption is the choice of either a single or two phase model. Some factors to be considered in comparing one and two phase models are:

(a) selection of a pseudohomogeneous temperature ($T^*$) within the range $T_f$ to $T_s$;
(b) selection of pseudohomogeneous heat transfer parameters $Pe_{hr}$ and $Bi_w$ to give the best approximation to the two phase radial heat transfer parameters;
(c) calculation of a nonisothermal effectiveness factor so that the pseudohomogeneous reaction rate equals the rate for the heterogeneous model:

$$\underset{\text{(one phase)}}{\eta^*(T^*, T_s - T_f)R_M(T^*)} = \underset{\text{(two phase)}}{\eta(T_s)R_M(T_s)}$$

(d) compensating for a slower secondary reaction rate (carbon monoxide production) for the single phase model if $T^* < T_s$, because the rates in the two phase model are based on $T_s$.

The comparison between the one and two phase models is little affected by axial heat transfer. However, the model comparison is complicated by the fact that radial heat transfer occurs in both the solid and the fluid phases for the two phase model rather than in the fluid phase only for the one phase model (see discussion in Pereira Duarte *et al.*, 1984a). To see these problems more clearly, let us consider the one dimensional energy balance given in Appendix B:

two phase:

$$\frac{dT_f}{dz} = St_h(T_s - T_f) + \alpha_f(T_w - T_f) \tag{36}$$

$$0 = St_h(T_f - T_s) + \alpha_s(T_w - T_s) + (1 - \varepsilon_b)B_R\bar{R}_e(T_s) \tag{37}$$

single phase:

$$\frac{dT^*}{dz} = \alpha(T_w - T^*) + (1 - \varepsilon_b)B_R\bar{R}_e(T^*) \tag{38}$$

If radial heat transfer is lumped in the fluid ($\alpha_f = \alpha$, $\alpha_s = 0$), then the proper selection of $T^*$ would be $T^* = T_f$. If there were equal heat transfer in solid and fluid ($\alpha_f = \alpha_s$), then $T^*$ could be chosen as

$$T^* = T_{avg} = (T_f + T_s)/2 \tag{39}$$

even though some mismatch would still exist due to

$$\frac{dT_f}{dz} \neq \frac{dT^*}{dz}. \tag{40}$$

Since the radial heat transfer rate in the fluid phase is approximately five times that in the solid, for the present case, we chose $T^* = T_f$.

For some special cases almost perfect matching can be achieved between the pseudohomogeneous and heterogeneous models. For example, if $T^* = T_f$ and there is no radial solid heat transfer ($\alpha_s = 0$), then the pseudohomogeneous heat transfer parameters are equal to those of the fluid: $Pe_{hr} = Pe_{fr}$ and $Bi_w = Bi_{wf}$. In this case, the one and two phase models are equivalent for a single reaction within the accuracy of the nonisothermal effectiveness factor representation for calculation of the pseudohomogeneous reaction rate. Similarly, in the limit of large interphase heat transfer ($St_h$ and $h_{fs} \to \infty$), then $T_f = T_s$ and $\alpha = \alpha_f + \alpha_s$, and the two model types are again equivalent.

However, for the realistic case of moderate interphase heat transfer resistance and radial transfer in the solid phase, the interphase catalyst temperature rise of the two phase model will be less than the temperature rise assumed in the nonisothermal effectiveness factor calculation of the single phase model. This is due to the presence of unmodelled heat losses of the solid particle to adjacent solid particles. Comparing terms of the one and two phase models:

$$\begin{aligned} &[St_h(T_s - T_f) = (1 - \varepsilon_b)B_R\bar{R}_e(T_s) - \alpha_s(T_s - T_w)] \text{ 2-phase} \\ &[St_h(T_s - T_f) = (1 - \varepsilon_b)B_R\bar{R}_e(T_s) \cong (1 - \varepsilon_b)B_R\bar{R}_e(T^*)] \text{ 1-phase} \end{aligned} \tag{41}$$

Thus, the pseudohomogeneous model has a higher reaction rate because $(T_s - T_f)_{\text{1-phase}} > (T_s - T_f)_{\text{2-phase}}$ which results in slightly higher reactor temperatures and conversions.

Note that the heat flux to the wall for the one phase and two phase models is given by:

$$q^{(1)} = \alpha(T^* - T_w); \qquad q^{(2)} = \alpha_f(T_f - T_w) + \alpha_s(T_s - T_w) \tag{42}$$

Now to compare them, let us assume the heat transfer coefficients are added ($\alpha = \alpha_f + \alpha_s$) and $T^* = T_f$; then the respective wall heat fluxes are:

$$q^{(1)} = (\alpha_f + \alpha_s)(T_f - T_w) \tag{43}$$

$$q^{(2)} = \alpha_f(T_f - T_w) + \alpha_s(T_f - T_w) + \alpha_s(T_s - T_f) \tag{44}$$

The single phase wall heat flux is less than that of the two phase model. To force equality of the heat flux for the two models, a varying overall coefficient must be used:

$$\alpha = \alpha_f + \alpha_s\left(\frac{T_s - T_w}{T_f - T_w}\right) \tag{45}$$

Thus it is difficult to exactly compare these models because one must make assumptions about parameters.

The differences between the one phase and two phase models are summarized in Table II together with proposed compensations to the single phase model. Based on our experience with the present system, these compensations can be very effective in matching the results of the two models. The extent of the maximum error in formaldehyde yield $(\Delta Y_F)_{\text{exit}}$ methanol concentration $(\Delta Y_M)_{\text{exit}}$

TABLE II

Effects of assumptions in the pseudohomogeneous model—comparison with heterogeneous model

| Effect | Cause | Results for single-phase model simulation compared to two-phase model | Suggested compensation within single-phase model |
|---|---|---|---|
| 1. $\bar{R}(T^*) \leq \bar{R}(T_s)$ | No explicit calculation of fluid and solid temperature and $T^* \leq T_s$ | $\begin{pmatrix} \Delta Y_{F_{exit}} = -8\% \\ \Delta T_{max} = -23°C \\ \Delta Y_{M_{exit}} = +18\% \end{pmatrix}$ | nonisothermal effectiveness factor so that $\eta^*(T^*, T_s - T_f)\, R(T^*) = \eta(T_s)\, R(T_s)$ |
| 2. $\frac{(T_s - T_f)_{1\text{-phase}}}{(T_s - T_f)_{2\text{-phase}}} > 1$ in effectiveness factor calculation | Conduction through solid phase in 2-phase model | | correlate larger apparent interphase heat transfer coefficient in single-phase model effectiveness factor |
| 3. $\frac{(\text{radial heat flux})_{1\text{-phase}}}{(\text{radial heat flux})_{2\text{-phase}}} < 1$ | Larger driving force for radial heat transfer in the solid phase than in a lumped phase because $T_s \geq T^*$ | $\begin{pmatrix} \Delta Y_{F_{exit}} = +2\% \\ \Delta Y_{M_{exit}} = +5\% \\ \Delta T_{max} = +9°C \end{pmatrix}$ | correlate larger apparent radial heat transfer in the 1-phase model |
| 4. $R_{CO}(T^*) \leq R_{CO}(T_s)$ lower secondary reaction rates | No explicit calculation of fluid and solid temperature and $T^* \leq T_s$ | $\begin{pmatrix} \Delta Y_{F_{exit}} = +0.2\% \\ \Delta Y_{M_{exit}} = -3\% \\ \Delta T_{max} = -7°C \\ \Delta Y_{CO_{exit}} = -20\% \end{pmatrix}$ | approximate $\Delta T = T_s - T_f$, then use $R_{CO} = f(T^*, \Delta T)$ OR adjust kinetics so that $k_{CO}$(1-phase) $> k_{CO}$(2-phase) |

CO formation $(\Delta Y_{co})_{exit}$ and temperature $(\Delta T)_{max}$ are indicated for the operating conditions and parameters given in Table I. In general,

$$\begin{pmatrix}\text{primary reaction}\\ \text{rate effects}\end{pmatrix} > \begin{pmatrix}\text{radial solid heat}\\ \text{transfer effects}\end{pmatrix} > \begin{pmatrix}\text{secondary reaction}\\ \text{rate effects}\end{pmatrix}$$

The primary reaction rate effects are proportional to the interphase temperature difference. The radial solid heat transfer effects are most significant at lower flow rates when the radial heat transfer through the solid ($\alpha_s$) is a significant fraction of overall radial heat transfer ($\alpha$). As $\alpha_s/\alpha$ becomes small (<0.1), then radial lumping of the fluid and solid is appropriate. The secondary reaction rate effects are most significant under conditions when the secondary reaction rate is substantial (>10% of products), when the secondary reaction is highly exothermic compared to primary reaction, or when the interphase temperature difference is large.

For the model comparisons presented in Figures 12–14 and in the dynamic simulation, only compensation in the effectiveness factor calculation (Effect #1 in

Table II) has been made. The differences due to the remaining effects can be seen in the figures. Since the solid and fluid temperatures differ by less than 15°C for the methanol oxidation reactor, only modest differences between the one and two phase models are observed. The main point of difference to be noted is that the pseudohomogeneous models give consistently higher reactor temperatures and formaldehyde yields. Reactor designs based on the pseudohomogeneous models indicate similar tube diameters and mass flow rates to the heterogeneous models but slightly underestimate the necessary tube length.

## DYNAMIC RESPONSE OF THE REACTOR MODEL

A study was made of model predictions of reactor dynamics for step changes in the operating variables. Figures 15–19 show the effects of step changes in wall temperature, feed temperature, feed mole fraction, and feed flow rate. These figures show the two steady state temperature and composition profiles and a few of the intermediate transient profiles for the two dimensional heterogeneous model. Another way to observe the dynamics is to plot in time the temperature and conversion at a particular location in the reactor and the yield and carbon monoxide production at the exit (Figures 20–23). These figures show comparisons of the different types of models.

A step increase in wall temperature (Figure 15) shows an overall increase in mean reactor temperature with subsequent increases at the hot spot. The temperature changes first near the wall (Figure 15b), and then a greater increase takes place in the interior of the reactor due to a large increase in reaction rate. The two dimensional model shows a delay in the centerline temperature response

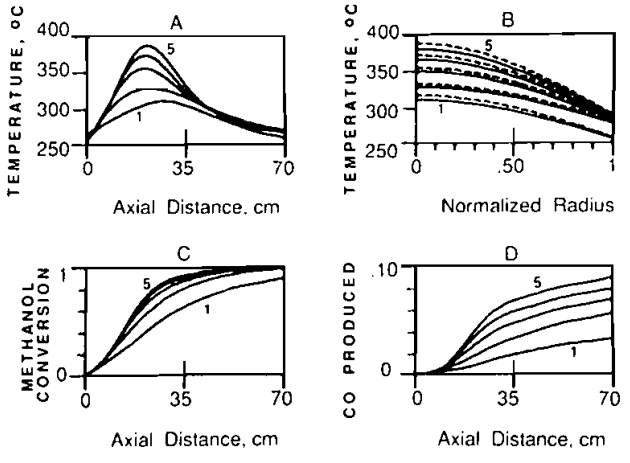


FIGURE 15 Reactor dynamics—Response to a step in wall temperature. 240 to 260 C. (1) Steady state @ 240 C; (2) 0.5 min; (3) 1.0 min; (4) 1.5 min; (5) Steady state @ 260 C. A: Centerline axial temperature profiles; B: Radial temperature profile at 25 cm; C: Axial methanol conversion profile; D: Axial profile of mole fraction carbon monoxide production.

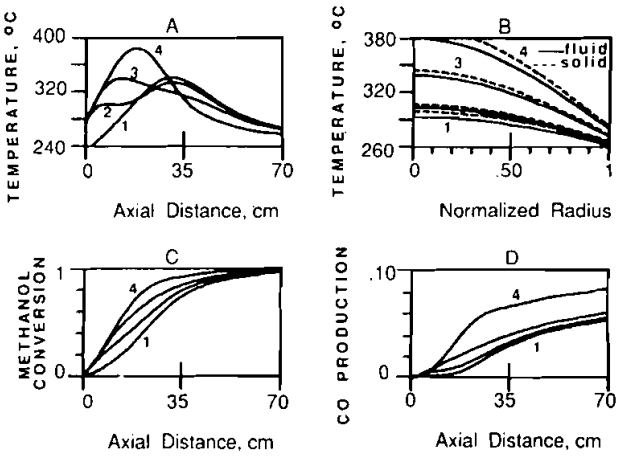


FIGURE 16 Reactor dynamics—Response to a step up in feed temperature. 230 to 270 C. (1) Steady state @ 230 C; (2) 0.5 min; (3) 1.0 min; (4) steady state @ 270 C. A: Centerline axial temperature profiles; B: Radial temperature profile at 15 cm; C: Axial methanol conversion profile; D: Axial profile of mole fraction carbon monoxide production.

(Figure 20a) which is more physically realistic than the immediate response of the radially lumped, one dimensional model. A transient maximum in yield occurs as the reactor temperature increases to, and passes through the conditions of maximum yield (Figure 20c). The carbon monoxide production (selectivity) is largely controlled by the hottest temperature region in the reactor, and so it responds somewhat more slowly than the methanol conversion (Figures 20b, 20d).

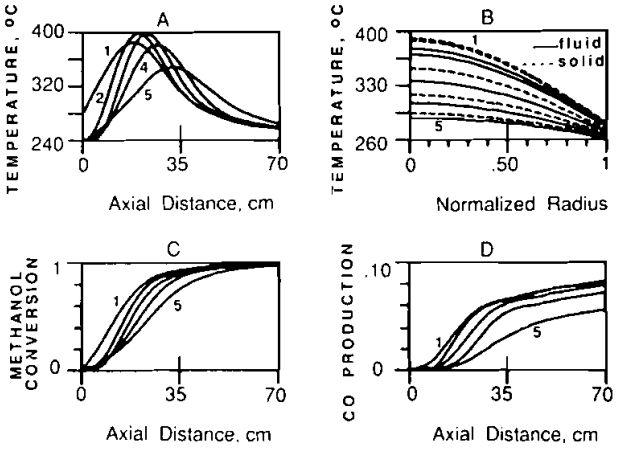


FIGURE 17 Reactor dynamics—Response to a step down in feed temperature. 270 to 230 C. (1) Steady state @ 270 C; (2) 0.5 min; (3) 1.0 min; (4) 1.5 min; (5) Steady state @ 230 C. A: Centerline axial temperature profiles; B: Radial temperature profile at 15 cm; C: Axial methanol conversion profile; D: Axial profile of mole fraction carbon monoxide production.

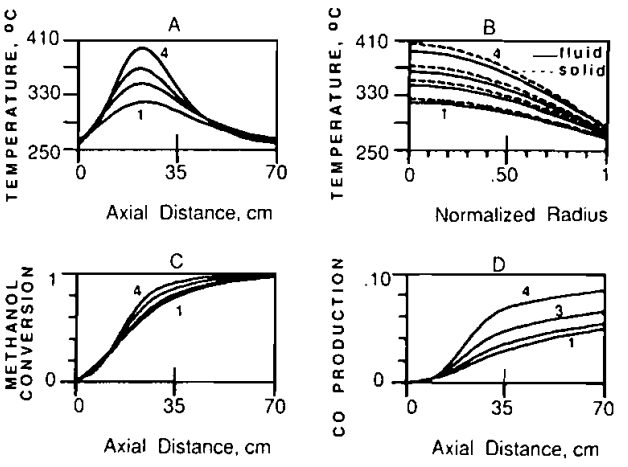


FIGURE 18 Reactor dynamics—Response to a step in methanol feed. 4% to 5%. (1) Steady state @ 4%; (2) 0.5 min; (3) 1.0 min; (4) steady state @ 5%. A: Centerline axial temperature profiles; B: Radial temperature profile at 25 cm; C: Axial methanol conversion profile; D: Axial profile of mole fraction carbon monoxide production.

For an increase in feed temperature (Figure 16), the initial decrease in hot spot temperature due to depletion of reactants is followed by the rapid development of a new hot spot closer to the reactor entrance. A decrease in feed temperature (Figure 17) results in a transient increase in the maximum reactor temperature as the hot spot moves downstream and then the temperature drops. The severe transient hot spot is due to increased methanol contacting the original reactor hot spot before it has been cooled by the lower temperature feed. This wrong-way

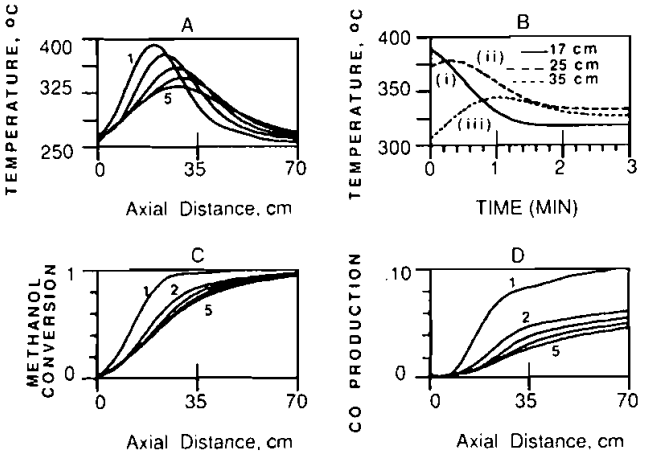


FIGURE 19 Reactor dynamics—Step increase in feed flow rate. 1.12 to 1.68 g/sec. (1) Steady state @ 1.12 g/sec; (2) 0.5 min; (3) 1.0 min; (4) 1.5 min; (5) Steady State @ 1.68 g/sec. A: Centerline axial temperature profiles; B: Centerline temperature at (i) ——— 17 cm, (ii) – – – – 25 cm, (iii) · · · · 35 cm; C: Axial methanol conversion profile; D: Axial profile of mole fraction carbon monoxide production.

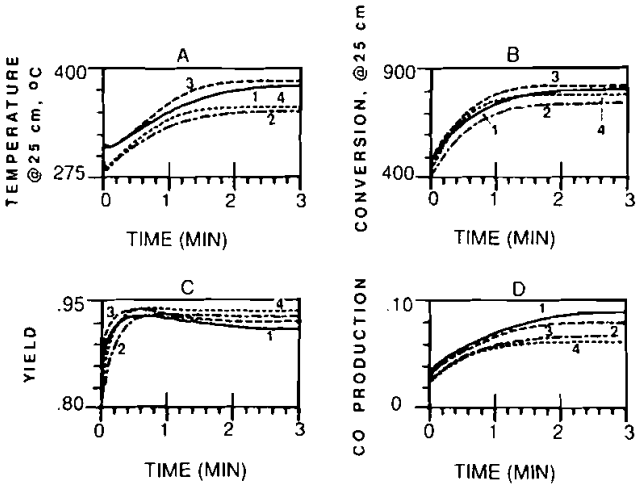


FIGURE 20 Reactor dynamics for wall temperature step, 240 to 260 C—Model comparison. (1) ——— 2-D heterogeneous; (2) · · · · 1-D heterogeneous; (3) – – – – 2-D pseudohomogeneous; (4) · · · · 1-D pseudohomogeneous. A: Centerline temperature at 25 cm; B: Methanol conversion at 25 cm; C: Yield; D: Mole fraction carbon monoxide production.

temperature response is more severe in the pseudohomogeneous model than the heterogeneous model (Figures 21a, 22a). Wrong-way behavior of the carbon monoxide production is shown by the two dimensional pseudohomogeneous model due to the large amount of wrong-way behavior in the hot spot temperature. If the heterogeneous model is used, the catalyst temperature near the entrance of the reactor will not change as rapidly as the pseudohomogeneous

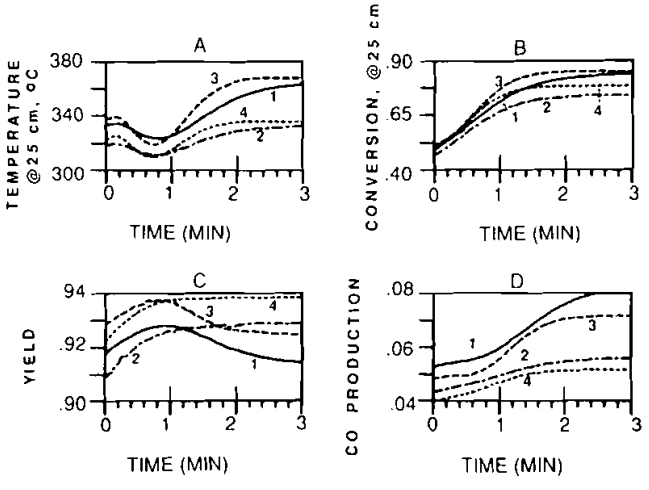


FIGURE 21 Reactor dynamics for feed temperature step, 230 to 270 C—Model comparison. (1) ——— 2-D heterogeneous; (2) · – · – 1-D heterogeneous; (3) – – – – 2-D pseudohomogeneous; (4) · · · 1-D pseudohomogeneous. A: Centerline temperature at 25 cm; B: Methanol conversion at 25 cm; C: Yield; D: Mole fraction carbon monoxide production.

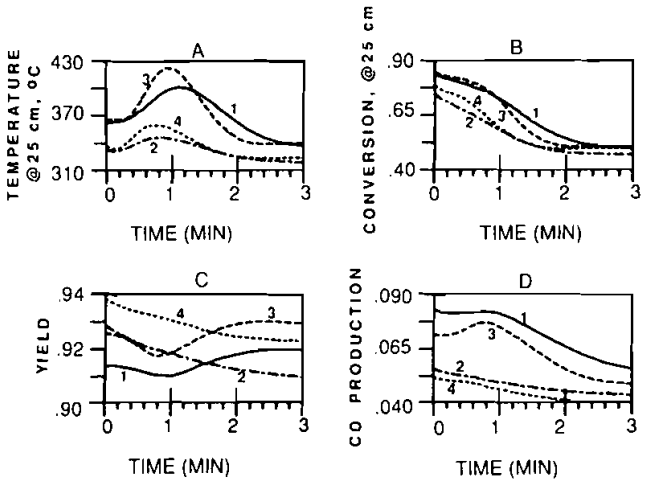


FIGURE 22 Reactor dynamics for feed temperature step, 270 to 230 C—Model comparison. (1) ——— 2-D heterogeneous; (2) · - · - 1-D heterogeneous; (3) – – – – 2-D pseudohomogeneous; (4) · · · · 1-D pseudohomogeneous. A: Centerline temperature at 25 cm; B: Methanol conversion at 25 cm; C: Yield; D: Mole fraction carbon monoxide production.

model temperature, which undergoes a step change. Therefore, the reactant stream contacting the reactor hot spot undergoes more severe transients in the single phase model. The response to feed temperature is generally slower than the response to wall temperature because changes must be propagated down the reactor bed rather than through the short distance from the wall toward the reactor centerline.

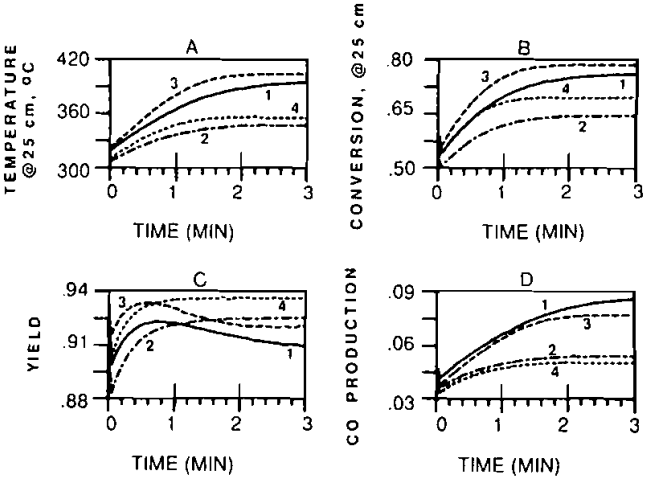


FIGURE 23 Reactor dynamics for methanol feed fraction step, 4% to 5%—Model comparison. (1) ——— 2-D heterogeneous; (2) · - · - 1-D heterogeneous; (3) – – – – 2-D pseudohomogeneous; (4) · · · · 1-D pseudohomogeneous. A: Centerline temperature at 25 cm; B: Methanol conversion at 25 cm; C: Yield; D: Mole fraction carbon monoxide production.

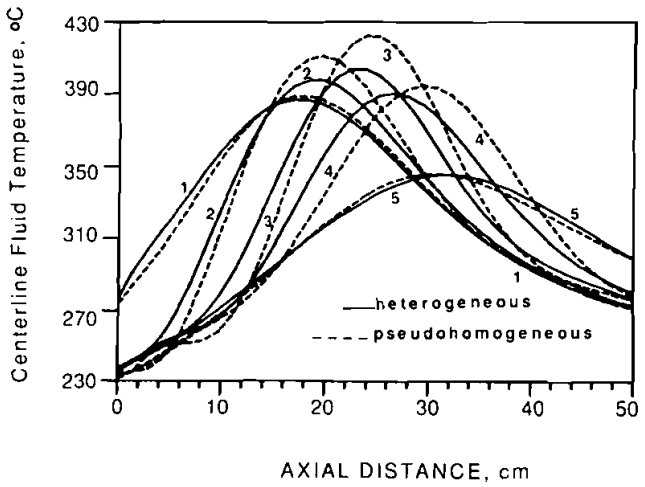


FIGURE 24 Comparison between one- and two-phase models—Centerline temperature profiles for a step decrease in feed temperature. 270 to 230 C. (1) Steady state at 270 C; (2) 0.5 min; (3) 1.0 min; (4) 1.5 min; (5) steady state at 230 C.

An increase in feed concentration (Figure 18) causes the temperatures to increase in the reactive region near the hot spot with little upstream or downstream shift. Figure 19 indicates the dynamics of an increase in feed flow rate including the appropriate changes in the transport parameters which depend on flow rate. Although the temperature profile shifts downstream, there is no increase in the maximum reactor temperature. Figure 19b indicates how different regions of the reactor show widely varying dynamic temperature responses such as wrong-way behavior and overshoot.

For all types of step changes considered, one and two dimensional models show similar qualitative behavior, but the two dimensional model is more sensitive, and external changes cause larger transients. However, the response of the two dimensional model is generally slower, due to the finite propagation speed of radial variations, particularly the radial temperature profile. Another major difference is that the two dimensional models often show transient maxima or minima in yield due to dynamic variations in reactor selectivity as the radial profiles develop (Figure 23). By contrast, the one dimensional models generally give a monotonic yield response.

The differences between the one and two phase models can be more important for dynamic responses than for steady state behavior. Even if the one and two phase models are matched for steady state conditions, the dynamic responses may not match. This is primarily due to the individual phases of the heterogeneous model correctly having transient deviations from the steady state catalyst particle temperature rise. A steady state interphase temperature rise is an assumption in the non-isothermal effectiveness factor calculation of the pseudohomogeneous model. An example is shown in Figure 24, which compares the temperature profiles of the heterogeneous and pseudohomogeneous models after a step

decrease in feed temperature (Figures 17, 22). The steady state agreement is good, but the transient profiles show significant differences in the fluid temperature.

## CONCLUSIONS

The dynamic simulation of a detailed packed bed reactor model on a mini-computer in less than real time is feasible. However, it is necessary to incorporate an efficient method for effectiveness factor calculations. The most important parameters for determination of reactor performance are the pre-exponential kinetic constant and the radial heat transport parameters. *A priori* correlations for these parameters are not sufficient for quantitative computations. The interphase heat transfer coefficient and wall Biot number show non-linear parametric sensitivity, but the methanol oxidation reactor operates in the region of low sensitivity to these parameters.

A detailed comparison has been made between the different types of models (one and two dimension, heterogeneous and pseudohomogeneous). The heterogeneous and pseudohomogeneous models show good qualitative agreement, particularly for moderate steady state conditions. The coincidence of the results from the two models could be made even better by parameter adjustment, such as in experimental parameter identification. The dynamic behavior of these two types of models is substantially different in some cases (such as in the case of axially travelling thermal waves), even if the steady states are similar. The source of differences between the one- and two-phase models has been analysed in a systematic manner, and methods to allow the pseudohomogeneous model to more accurately mimic a heterogeneous model have been given.

The one dimensional and two dimensional models show different hot spot sensitivity and different yield maxima positions. The two dimensional model is much more effective than the one dimensional model in predicting decreases in selectivity due to excessive hot spot temperatures. For conditions less severe than the "optimal yield point" the one and two dimensional models give similar dynamic responses.

Both steady state and dynamic effects of the operating conditions have been investigated. The wall temperature has a much greater effect on reactor behavior than the feed temperature. However, while the steady state yield declines slowly as the feed temperature is decreased, reactor runaway can occur at excessive feed temperatures. In addition, significant wrong-way behavior can occur for feed temperature changes. These are especially undesirable for feed temperature decreases which produce large transient increases in the maximum reactor temperature. High yields are obtained for all methanol feed mole fractions in the range of 0.01 to 0.05. However, there is a distinctive yield minimum at ~3% methanol feed concentration, making the methanol-rich feeds more desirable. Although feeds with more than 5–6% methanol offer increased productivity, they can lead to less selectivity by creating an excessive temperature rise within the reactor, and are in close proximity to the explosive regime of methanol-air

mixtures. Thus good safety practice and process control are essential for the higher methanol concentrations. Feed flow rate variations shift the reaction zone in the axial direction, and can be used to adjust performance to account for catalyst activity and reactor length. No wrong-way behavior in the reactor maximum temperature is observed for step changes in the flow rate.

## ACKNOWLEDGEMENTS

The authors are indebted to the National Science Foundation, the Department of Energy, and the DuPont Company for support of this research.



## NOMENCLATURE

| | |
|---|---|
| A | $L/r_t$ |
| $A_j$ | Arrhenius frequency factor for reaction $j$ |
| $B_C$ | matrix for particle collocation solution |
| $B_R$ | dimensionless reactor temperature rise, $= -\Delta HR_0L/FT_0$ |
| $Bi$ | Biot number |
| $c$ | Concentration |
| $C_p$ | heat capacity |
| $d$ | diameter |
| $d_0$ | outside cylinder diameter |
| $d_i$ | inside hole diameter of hollow cylinder |
| $d_s$ | diameter of surface-equivalent sphere |
| $d_x$ | diameter of sphere with same volume to external surface ratio |
| $d_c$ | diameter of volume-equivalent sphere w.r.t. a solid cylinder |
| $d_{sz}$, $d_{sr}$, $d_{fz}$, $d_{fr}$, $d_{yz}$ | vectors of boundary collocation terms |
| $D_e$ | effective diffusivity |
| $D_r$ | effective radial dispersion coefficient |
| $D_z$ | effective axial dispersion coefficient |
| $Da$ | dimensionless Damkohler number, $= R_{mo}LM_w/G_0$ |
| $E$ | dimensionless, $E^2 = \exp(\gamma(1 - 1/\Theta))$ |
| $E_j$ | activation energy for reaction $j$ |
| $F$ | thermal velocity, $= (v\rho C_p)_f$ |
| $G$ | mass velocity, $= (v\rho)_f$ |
| $h$ | two phase heat transfer coefficient |
| $\Delta H_j$ | heat of reaction $j$ |

| | |
|---|---|
| $k$ | thermal conductivity |
| $k_j$ | rate constant for reaction $j$, $= A_j \exp(E_j/R_g T)$ |
| $k_m$ | catalyst-fluid film mass transfer coefficient |
| $K_j$ | adsorption constant of component $j$ |
| $K_a$ | redox kinetic constant incorporating oxidation and reduction rates; analogous to MeOH adsorption term |
| $l_p$ | length of cylindrical pellet |
| $L$ | length of reactor |
| $Le$ | Lewis number, ratio of fluid to solid heat capacity |
| $Le_p$ | Lewis number for catalyst particle |
| $m$ | mass flow rate |
| $M_w$ | molecular weight of reaction mixture |
| $n$ | reaction order |
| $N_r$ | parameter for heat transfer ~125 |
| $NP$ | number of collocation points in the catalyst particle |
| $N_R$ | number of radial interior collocation points |
| $N_Z$ | number of axial interior collocation points |
| $P_j$ | partial pressure of component $j$, $= y_j P_T$ |
| $Pe$ | Peclet number based on reactor length or radius |
| $Pe'$ | Peclet number based on catalyst diameter |
| $P_T$ | total reactor pressure |
| $q_i$ | vector of constants in collocation formulation for catalyst particle |
| $r_t$ | radius of reactor |
| $R_e$ | effective rate of methanol reaction which would release the equivalent heat as the sum of all reactions occuring |
| $R_g$ | gas constant |
| $\bar{R}_j$ | dimensionless effective rate of reaction for component $j$, $= (\eta_j R_j)/R_0$ |
| $R_j$ | rate of disappearance by reaction for component $j$, based on catalyst volume, (mol/s cm$^3$cat atm) |
| $Re$ | Reynolds number, based on particle diameter |
| $S_v$ | external surface of catalyst per volume reactor |
| $St$ | Stanton number |
| $St'$ | Stanton number based on particle diameter |
| $t$ | time |
| $T$ | temperature |
| $U$ | overall heat transfer coefficient |
| $v$ | superficial velocity |

$W_k$ interpolation weights

$W_{sz}$, $W_{sr}$, $W_{fz}$, $W_{fr}$, $W_{yz}$, $W_{yr}$ matrices of collocation constants

$x$ catalyst particle coordinate

$y_i$ mole fraction of component $i$, $= C' R_g T$

$Y'$ partial pressure dependency of reaction rate, $= R'_m / k_1$

$Y$ dimensionless partial pressure, $= Y'/Y_0$

*Greek Letters*

$\beta$ dimensionless adiabatic temperature rise in catalyst, $= -\Delta H D_e C_f / \lambda T_f$

$\gamma$ dimensionless activation energy, $= E_1 / R_g T_f$

$\varepsilon$ void fraction

$\eta$ effectiveness factor

$\theta$ dimensionless temperature inside catalyst, $= (T_s / T_f)$

$\lambda$ effective thermal conductivity of catalyst particle

$\mu_0$, $\mu_1$ axial solid boundary condition terms

$\rho$ density

$\tau_p$ dimensionless time for catalyst particle, $= 4 D_e t / d_x^2 \varepsilon_p$

$\tau_r$ dimensionless time for reactor

$\phi$ Thiele modulus, $= d_x / 2 (R_0 / D_e C_0)^{0.5}$

$\psi_0$, $\psi_1$ axial fluid boundary condition terms

*Subscripts*

$b$ bed of reactor

$CO$ carbon monoxide

$e$ effective

$ex$ at reactor exit

$f$ fluid phase

$F$ formaldehyde

$h$ heat transfer

$i$ at reactor inlet

$m$ mass transfer

$M$ methanol

$o$ reference

$O$ oxygen

$p$ catalyst particle

$qs$ by radiation between solid surfaces

| | |
|---|---|
| $qv$ | by radiation in the voids |
| $r$ | radial |
| $s$ | solid phase |
| $t$ | reactor tube |
| $u$ | at the catalyst surface |
| $w$ | at the reactor wall |
| $x$ | particle coordinate (spherical) |
| $z$ | axial |



## REFERENCES


Amundson, N.R., *Berichte der Bunsen-Gesellschaft*, **2,** 90–98 (1970).
Bauer, R., and Schlunder, E.U., *Int. Chem. Eng.*, **18,** 181–188 (1978a).
Bauer, R., and Schlunder, E.U., *Int. Chem. Eng.*, **18,** 189–204 (1978b).
Bibin, B.V., and Popov, B.I., *Kinetics and Catalysis*, **10,** 1091–1098 (1969).
Byrne, G.D., Hindmarsh, A.C., *ACM Trans. on Mathematical Software*, **1,** 71–96 (1975).
Carberry, J.J., *Trans. Instn. Chem. Engs.*, **59,** 75–82 (1981).
Cresswell, D.L., and Dixon, A.G., *AIChE J.* **28,** 511–513 (1982).
Dente, M., Biardi, G., and Ranzi, E., Proc. 5th Europ./2nd Int. Symp. Chem. React. Eng., Amsterdam, B5: 13–22 (1972).
Dente, M., and Collina, A. *La Chimica e L'Industria*, **47,** 821–829 (1965).
Dente, M., Collina, A., and Pasquon, I. *La Chimica et L'Industria* 1966, **48,** 581–588.
Dente, M., and Pasquon, I., *La Chimica e L'Industria*, **47,** 359–267 (1965).
Dente, M., Poppi, R., and Pasquon, I., *La Chimica e L'Industria*, **47,** 1326–1337 (1964).
DeWasch, A.P., and Froment, G.F., *Chem. Eng. Sci.* **27,** 567–576 (1972).
Dixon, A.G., and Cresswell, D.L., *AIChE J.* **25,** 663–676 (1979).
Dixon, A.G., and Paterson, W.R., and Creswell, D.L., *ACS Symposium Series* (*Proc. 5th ISCRE, Houston, TX*) **65,** 238–253 (1978).
Emig, G., Hofmann, M., and Friedrich, H. Proc. 5th Europ./2nd Int. Symp. Chem. React. Eng., Amsterdam, B5: 23–38 (1972).
Finlayson, B.A., *Chem. Eng. Sci.*, **26,** 1081–1091 (1971).
Finalyson, B.A., *The Method of Weighted Residuals and Variational Principles*, Ch. 5: Chemical Reaction Systems, Academic Press: New York, 1972.
Finlayson, B.A., *Cat. Rev.–Sci. Eng.* **10(1),** 69–138. (1974)
Froment, G.F., Proc. 5th Europ./2nd Int. Symp. Chem. React. Eng., Amsterdam, A5: 1–20 (1972).
Froment, G.F., and Bischoff, K.B., *Chemical Reactor Analysis and Design*, Wiley: New York, NY, 1979.
Gunn, D.J., and DeSouza, J.F., *Chem. Eng. Sci.* **29,** 1363–1371 (1974).
Gunn, D.J., and Khalid, M. *Chem. Eng. Sci.*, **30,** 261–267 (1975).
Hansen, K.W., *Chem. Eng. Sci.* **26,** 1555–1569 (1971).
Hlavacek, V., *Ind. Eng. Chem.* **62(7),** 8–26 (1970).
Jiru, P., Tichy, J., and Wichterlova, B., *Collect. Czech. Chem. Commun.*, **31,** 674–688 (1966).
Jiru, P., Wichterlova, B., and Tichy, J., 3rd Int. Cong. Catal., Amsterdam, 199–213 (1964).
Karanth, N.G., and Hughes, R. *Chem. Eng. Sci.* **29,** 197–205 (1974a).
Karanth, N.G., and Hughes, R., *Cat. Rev.–Sci. Eng.*, **9,** 169–208 (1974b).
Kulkarni, B.D., and Doriaswamy, L.K., *Cat. Rev.–Sci. Eng.*, **22,** 431–483 (1980).
Li, C.H., and Finlayson, B.A., *Chem. Eng. Sci.* **32,** 1055–1066 (1977).
Machiels, C.J., *Catalysis Under Transient Conditions–ACS Symp. Ser.* **178,** 238–251 (1982).
Machiels, C.J., and Sleight, A.W., Proc. 4th Int. Conf. on the Chemistry and Uses of Molybdenum, Golden, CO, 411 (1982).
Mars, P., and Van Krevelen, D.W., *Chem. Eng. Sci.* (*Special Supplement*) **3,** 298–314 (1954).
Olbrich, W.E., and Potter, O.E., *Chem. Eng. Sci.* **27,** 1733–1743 (1972).

Panthel, G., Ph.D. Dissertation, Univ. Erlangen–Nurnberg, West Germany, 1977.
Pereira Duarte, S.I., Barreto, G.F., and Lemcoff, N.O. *Chem. Eng. Sci.* **39,** 1017–1024 (1984a).
Pereira Duarte, S.I., Ferretti, O.A., and Lemcoff, N.O., *Chem. Eng. Sci.* **39,** 1025–1031 (1984b).
Pernicone, N., Lazzerin, F., and Lanzavecchia, G., *J. Catalysis* **10,** 83 (1968).
Pernicone, N., Lazzerin, F., Liberti, G., and Lanzavecchia, G. *J. Catalysis* **14,** 293–302 (1969).
Santacesaria, E., Morbidelli, M., and Carra, S., *Chem. Eng. Sci.* **36,** 909–917 (1981).
Schlunder, E.U., 5th Int. Symp. Chem. React. Eng. Reviews, Houston, TX, 111–161 (1978).
Schwedock, M.J., Ph.D. Dissertation, Univ. of Wisconsin, Madison, (1983).
Specchia, V., Baldi, G., and Sicardi, S., *Chem. Eng. Comm.* **4,** 361–380 (1980).
Villadsen, J.V., and Stewart, W.E., *Chem. Eng. Sci.*, **22,** 1483–1501 (1967).
Vortmeyer, D., *Germ. Chem. Eng.* **3,** 124–138 (1980).
Vortmeyer, D., and Berninger, R. *AIChE J.* **28,** 508–510, 525 (1982).
Vortmeyer, D., and Schaeffer, R.J., *Chem. Eng. Sci.* **29,** 485–491 (1974).
Votruba, J., Hlavacek, V., and Marek, M., *Chem. Eng. Sci.* **7,** 1845–1851 (1972).
Wheeler, A., *Advances in Catalysis* **3,** 249 (1957).
Windes, L.C., Ph.D. Dissertation, Univ. of Wisconsin, Madison, 1986.
Yagi, S., and Kunii, D., *AIChE J.* **6,** 373–381 1960.
Yagi, S., and Wakao, N. *AIChE J.* **5,** 79–85 1959.
Young, L.C., and Finlayson, B.A., *Ind. Eng. Chem. Fundam.* **12(4),** 412–422 (1973).



# APPENDIX A
## HEAT TRANSFER PARAMETER CORRELATIONS

A. Solid-Fluid Interphase Heat Transfer Coefficient (Fig. 3.2.b-1 Froment and Bischoff, 1979)

$$Nu_p = h_{fs}\, d_s/k_f = 1.27\, Pr^{1/3}\, Re^{0.56} = 32 \tag{A1}$$

B. Solid Phase Conductivity (Bauer and Schlunder, 1978b)

$$\text{Shape factors: } C_c = 2.5(1 + (d_i/d_0)^2) = 2.9$$

$$d_c = d_0(3l/2\, d_0)^{1/3} = 0.46 \text{ cm}$$

$$B_c = C_c \frac{(1-\varepsilon_b)^{10/9}}{\varepsilon_b} \tag{A2}$$

$$\text{Radiation: } N_r = k_{qs}/k_f = 4\sigma_{SB}\zeta T^3\, d_c/k_f = 4.2 \tag{A3}$$

$$\text{Radiative Transfer Factor: } \zeta = e \simeq 0.8$$

(see Vortmeyer, 1980 tables 1 & 2 for alternatives)

$$\text{Stefan–Boltzman constant: } \sigma_{SB} = 5.67 \times 10^{-8}\, W/m^2 - K^4$$

$$X \equiv \lambda_e/k_f = 8; \qquad P \equiv 1 + N_r/X - B_c/X = 1.16$$

$$\frac{k_s}{k_f} = (1-\varepsilon_b)^{1/2}\frac{2}{p}\left[\left(\frac{B_c(1 + N_r/X - 1/X)}{P^2}\right)\ln\left(\frac{X + N_r}{B_c}\right) - \frac{B_c - 1}{P} + \frac{B_c + 1}{2B_c}(N_r - B_c)\right] = 4.4 \tag{A4}$$

C. Fluid Radial Thermal conductivity

Stagnant Fluid Conductivity: $k_{ef^0}$

$$\text{Geometric model: } k_{ef^0}/k_f = (1 + \varepsilon_b N_r)(1 - (1 - \varepsilon_b)^{1/2}) = 1 \tag{A5}$$

$$\text{Series-Parallel: } k_{ef^0}/k_f = \varepsilon_b(1 + 0.72 k_{qv}/k_f) = 2.2 \tag{A6}$$

$$\frac{k_{qv}}{k_f} = 4\sigma_{SB} T^3 d_c \Big/ \left(1 + \frac{\varepsilon_b}{2(1-\varepsilon_b)}\left(\frac{1-e}{e}\right)\right) k_f = 4.7 \tag{A7}$$

Convective Transport Coefficient: $k_{fr^d}$ (Bauer and Schlunder, 1978a)

$$\text{Mixing length} = L_f = \Delta\psi F_c d_c + (1 - \Delta\psi) F_h d_h \tag{A8}$$

$$\psi_h = \psi_c + (1 - \psi_c)(d_i/d_0)^2; \qquad D \equiv (d_i/d_0)^2$$

$$\Delta\psi = \psi_c/\psi_h = (1 - D/\psi_h)/(1 - D) = 0.815 \tag{A9}$$

$$F_c = 1.75 \quad F_h = 2.8 \quad d_h = (2L^2)^{1/2} = 0.495 \text{ cm}$$

$$L_f = 0.91 \text{ cm}$$

$$Pe^*_{fr} = GC_p L_f / k_{fr^d} = K \quad \text{or} \quad \frac{k_{fr^d}}{k_f} = \frac{GC_p L_f}{K k_f} = 34.3 \tag{A10}$$

$$K = 8(2 - (1 - d_s/r_t)^2) = 13.2 \tag{A11}$$

$$k_{fr} = k_{ef^0} + k_{fr^d} \tag{A12}$$

$$k_{fr}/k_f = 36; \qquad Pe'_{fr} = 6.4$$

D. Overall Effective Radial Thermal conductivity

$$\frac{1}{Pe'_{hr}} = \frac{1}{Pe'_{fr}} + \frac{1}{Pe'_{sr}} \left| \frac{(Bi_{wf} + 4)/B_{iwf}}{8/N_s + (Bi_{ws} + 4)/Bi_{ws}} \right| = 0.197 \tag{A13}$$

$$N_s = \frac{6(1 - \varepsilon_b)(r_t/d_c)^2}{\frac{k_s}{k_f}\left(\frac{1}{Nu_p} + \frac{0.125}{X}\right)} = 125 \quad \text{(Dixon and Cresswell, 1979)} \tag{A14}$$

E. Wall Heat Transfer

Method A: from Specchia *et al.*, 1980

$$Nu_w = \frac{h_w d_c}{k_f} = \frac{h_{w^0} d_c}{k_f} + \frac{h_{w^d} d_c}{k_f} = Nu_{w^0} + H_w Re^n \tag{A15}$$

$$Nu_{w^0} = \varepsilon_b(2 + k_{qv}/k_f) + (1 - \varepsilon_b) \Big/ \left(\frac{1}{1/\delta_w + k_{qs}/k_f} + \frac{\gamma_w}{X}\right) \tag{A16}$$

$$\gamma_w = 0.14 \quad \delta_w = 0.0024(d_t/d_v)^{1.58} = 0.043$$

Constants:

| Reference | $H_w$ | $n$ | $Nu_{w^0}$ |
|---|---|---|---|
| Li and Finlayson, 1977 | 0.16 | 0.93 | no |
| Specchia *et al.*, 1980 | 0.084 | 0.91 | yes |
| Gunn and Khalid, 1975 | 4.2 | 0.475 | no |
| DeWasch and Froment, 1972 | 0.066 | 1.0 | yes |

Method B: Compute wall-fluid and wall solid coefficients

$$Nu_{wf} = \frac{h_{wf}\, d_c}{k_f} = H_{wf}\, Pr^{1/3}\, Re^{p} \tag{A17}$$

$$Bi_{wf} = \frac{Nu_{wf}\, Pe_{fr}}{Re\, Pr} = Pe_{fr} H_{wf}\, Pr^{-2/3}\, Re^{(p-1)} \tag{A18}$$

Constants:

| Reference | $H_{wf}$ | $p$ |
|---|---|---|
| Yagi and Wakao, 1959 | 0.2 | 0.8 |
| Dixon and Cresswell, 1979 | $0.06/\varepsilon_W^2$ | 0.75 |
| Olbrich and Potter, 1972 | 8.9 | 0.34 |

Wall-Solid Heat Transfer Coefficient

$$h_{ws} = 2.12\, k_{rs}/d_c; \quad Bi_{ws} = 1.06\, d_t/d_c = 6. \tag{A19}$$

(Dixon and Cresswell, 1979)

Overall Wall Heat Transfer Coefficient

$$Nu_w = 8\Psi(d_c/d_t) + Nu_{wf}\left(1 + \Psi \frac{Pe'_{fr}}{Re\, Pr}\right); \qquad Nu_{wf} \simeq 35 \tag{A20}$$

$$\Psi = \frac{k_s/k_f}{8/N_s + (Bi_{ws} + 4)/Bi_{ws}} = 2.5 \quad \text{(Dixon and Cresswell, 1979)}$$

Method C: Direct correlation of Biot number

$$Bi_w = 5.3(d_t/d_c)^{1/2}\, Re^{-0.262} = 2.8 \quad \text{(Dixon } et\ al.\text{, 1978)} \tag{A21}$$

# APPENDIX B
## MODEL EQUATIONS

A. Two-Dimensional Pseudohomogeneous Model

mass:

$$0 = \frac{1}{Pe_{mz}} \frac{\partial^2 y_j}{\partial z^2} + \frac{a}{Pe_{mr}} \frac{1}{r}\left(\frac{\partial}{\partial r} r \frac{\partial y_j}{\partial r}\right) - \frac{\partial y_j}{\partial z} - (1 - \varepsilon_b) Da \bar{R}_j(p_j, T) \tag{B1}$$

energy:

$$Le^* \frac{\partial T}{\partial \tau_r} = \frac{1}{Pe_{hz}} \frac{\partial^2 T}{\partial z^2} + \frac{a}{Pe_{hr}} \frac{1}{r} \left( \frac{\partial}{\partial r} r \frac{\partial T}{\partial r} \right) - \frac{\partial T}{\partial z} + (1 - \varepsilon_b) B_R \bar{R}_e \tag{B2}$$

Boundary Conditions:

$$r = 0 \qquad \frac{\partial T}{\partial r} = \frac{\partial y}{\partial r} = 0 \tag{B3}$$

$$r = 1 \qquad \frac{\partial T}{\partial r} = Bi_w (T_w - T); \qquad \frac{\partial y_j}{\partial r} = 0 \tag{B4}$$

$$z = 0 \qquad \frac{\partial T}{\partial z} = Pe_{hz} \frac{1}{2} (1 + \sigma^*)(T - T_i); \qquad \frac{\partial y_j}{\partial z} = Pe_{mz} (y - y_i) \tag{B5}$$

$$z = 1 \qquad \frac{\partial T}{\partial z} = Pe_{hz} \frac{1}{2} (1 - \sigma^*)(T - T_w); \qquad \frac{\partial y_j}{\partial z} = 0 \tag{B6}$$

$$\sigma^* = \left[ 1 + \frac{24 Bi_w a}{Pe_{hr}\, Pe_{hz} (Bi_w + 3)} \right]^{1/2} \tag{B7}$$

B. One-Dimensional Pseudohomogeneous Model

mass:

$$0 = \frac{1}{Pe_{mz}} \frac{\partial^2 y_j}{dz^2} - \frac{\partial y_j}{\partial z} - (1 - \varepsilon_b) Da \bar{R}_j (p_j, T) \tag{B8}$$

energy:

$$Le^* \frac{\partial T}{\partial \tau_r} = \frac{1}{Pe_{hz}} \frac{\partial^2 T}{\partial z^2} - \frac{\partial T}{\partial z} + (1 - \varepsilon_b) B_R \bar{R}_e + \alpha (T_w - T) \tag{B9}$$

Boundary Conditions:

$$z = 0 \qquad \frac{\partial T}{\partial z} = Pe_{hz} (T - T_i); \qquad \frac{\partial y}{\partial z} = Pe_{mz} (y - y_i) \tag{B10}$$

$$z = 1 \qquad \frac{\partial T}{\partial z} = \frac{\partial y}{\partial z} = 0 \tag{B11}$$

C. One-Dimensional Heterogeneous Model

mass:

$$0 = \frac{1}{Pe_{mz}} \frac{\partial^2 y_j}{\partial z^2} - \frac{\partial y_j}{\partial z} - (1 - \varepsilon_b) Da \bar{R}_j (p_j, T_s) \tag{B12}$$

energy:

(fluid):

$$0 = \frac{1}{Pe_{fz}} \frac{\partial^2 T_f}{\partial z^2} - \frac{\partial T_f}{\partial z} + St_h (T_s - T_f) + \alpha_f (T_w - T_f) \tag{B13}$$

(solid):

$$Le\frac{\partial T_s}{\partial \tau_r}=\frac{1}{Pe_{sz}}\frac{\partial^2 T_s}{\partial z^2}+St_h(T_f-T_s)+(1-\varepsilon_b)B_R\bar{R}_e+\alpha_s(T_w-T_s) \tag{B14}$$

Boundary Conditions:

$$z=0 \qquad \frac{\partial y}{\partial z}=Pe_{mz}(y-y_i); \qquad \frac{\partial T_f}{\partial z}=Pe_{fz}(T_f-T_i); \qquad \frac{\partial T_s}{\partial z}=0 \tag{B15}$$

$$z=1 \qquad \frac{\partial y}{\partial z}=\frac{\partial T_f}{\partial z}=\frac{\partial T_s}{\partial z}=0 \tag{B16}$$

The dimensionless quantities not previously defined are:

$$Le^*=\frac{\varepsilon_b(\rho C_p)_f+(1-\varepsilon_b)(\rho C_p)_s}{(\rho C_p)_f}$$
$$Pe_{hz}=\frac{GC_{pf}L}{k_{ez}} \qquad Pe_{hr}=\frac{GC_{pf}r_t}{k_{er}} \qquad Bi_w=\frac{h_w r_t}{k_{er}} \tag{B17}$$

Using a one point collocation approximation at $r=0.707$, the dimensionless overall heat transfer parameter is:

$$\alpha=\frac{2UL}{Fr_t}=\frac{2L}{r_t\,Pe_{hr}}\left[\frac{4Bi_w}{Bi_w+4}\right]$$
$$\alpha_f=\frac{2L}{r_t\,Pe_{fr}}\left[\frac{4Bi_{wf}}{Bi_{wf}+4}\right] \qquad \alpha_s=\frac{2L}{r_t\,Pe_{sr}}\left[\frac{4Bi_{ws}}{Bi_{ws}+4}\right] \tag{B18}$$

# APPENDIX C
## COLLOCATION EQUATIONS FOR THE TWO DIMENSIONAL HETEROGENEOUS REACTOR MODEL

$$Le\frac{dT_{s,ij}}{d\tau_r}=\sum_{k=1}^{NZ}W_{sz,jk}T_{s,ik}+\sum_{k=1}^{NR}W_{sr,ik}T_{s,kj}+d_{sz,j}+d_{sr,i}$$
$$+St_h(T_{f,ij}-T_{s,ij})+(1-\varepsilon_b)B_R\bar{R}_{e,ij} \tag{C1}$$

$$0=\sum_{k=1}^{NZ}W_{fz,jk}T_{f,ik}+\sum_{k=1}^{NR}W_{fr,ik}T_{f,kj}+d_{fz,j}+d_{fr,i}+St_h(T_{s,ij}-T_{f,ij}) \tag{C2}$$

$$0=\sum_{k=1}^{NZ}W_{yz,jk}y_{M,ik}+\sum_{k=1}^{NR}W_{yr,ik}y_{M,kj}+d_{yz,j}-(1-\varepsilon_b)Da\bar{R}_{M,ij} \tag{C3}$$

$$0=\sum_{k=1}^{NZ}W_{yz,jk}y_{CO,ik}+\sum_{k=1}^{NR}W_{yr,ik}y_{CO,kj}+d_{yz,j}+(1-\varepsilon_b)Da\bar{R}_{CO,ij} \tag{C4}$$

where $j=1,\ldots,NZ$; $i=1,\ldots,NR$.